https://doi.org/10.5194/acp-2020-481
Preprint. Discussion started: 29 July 2020

Atmospheric Chemistry and Physics Discussions

Changing characteristics of atmospheric CH_4 on the Tibetan Plateau, records from 1994 to 2017 at Mount Waliguan station

Shuo Liu[1,2,3], Shuangxi Fang[3], Peng Liu[4], Miao Liang[5], Minrui Guo[6], Zhaozhong Feng[1,7]

[1]State Key Laboratory of Urban and Regional Ecology, Research Center for Eco-Environmental Sciences, Chinese Academy of Sciences, Beijing, China

[2]College of Resources and Environment, University of Chinese Academy of Sciences, Beijing, China

[3]College of Environment, Zhejiang University of Technology, Hangzhou, China

[4]Mt. Waliguan background station, China Meteorological Administration (CMA), Qinghai, China

[5]Meteorological Observation Center (MOC), China Meteorological Administration (CMA), Beijing, China

[6]College of Global Change and Earth System Science, Beijing Normal University, Beijing, China

[7]Institute of Ecology, Key Laboratory of Agrometeorology of Jiangsu Province, School of Applied Meteorology, Nanjing University of Information Science & Technology, Nanjing, China

Correspondence:

Shuangxi Fang (fangsx@cma.gov.cn); Zhaozhong Feng (zhzhfeng201@hotmail.com)

https://doi.org/10.5194/acp-2020-481
Preprint. Discussion started: 29 July 2020

Atmospheric Chemistry and Physics Discussions

Abstract. A 24-year long-term observation of atmospheric CH_4 was presented at Mt.Waliguan (WLG) station, the only WMO/GAW global station in inland of Eurasia. Overall, during 1994-2017, continuously increase of atmospheric CH_4 was observed at WLG with yearly growth rate of 5.1 ± 0.1 ppb yr^{-1}, although near-zero and even negative growth appeared in some particular periods, e.g., 1999-2000, and 2004-2006. The average CH_4 mole fraction was only 1805.8 ± 0.1 ppb in 1995, but unprecedented elevated ~100 ppb and reached a historic high of 1903.8 ± 0.1 ppb in 2016. The seasonal averages of atmospheric CH_4 at WLG were ordered by summer, winter, autumn and spring, and the correlation slopes of $\Delta CO/\Delta CH_4$ showed a maximum in summer and minimum in winter, which was almost opposite to other sites in the northern hemisphere, e.g., Mauna Loa, Jungfraujoch, and was caused by regional transport. Strong potential sources at WLG were predominately identified in northeast (cities, e.g., Xining, Lanzhou) and southwest (the Northern India), and air masses from west and northwest regions were accompanied with higher CH_4 mole fractions than that from city regions.

What is interesting is that obviously changes appeared in different observing periods. Generally, i) the amplitudes of diurnal or seasonal cycles were continuously increasing over time, ii) the wind sectors with elevated CH_4 moved from ENE-…-SSE sectors in early periods to NNE-…-E sectors (city regions) in later years, iii) the area of source regions was increasing along with the years, and strong sources gradually shifted from northeast to southwest, iv) the annual growth rates in recent years (e.g., 2013-2016) were significantly larger than that in early periods (e.g., 1998-2012). We conclude that the site was more and more affected by regional sources along with the time. Northern India was possibly becoming the strongest source area to WLG rather than city regions before. The case study in the Tibetan Plateau showed that the atmospheric CH_4 observed in Qinghai-Tibetan Plateau changed not as expected, the annual growth rate was even larger than that in city regions in some period (e.g., 7.3 ± 0.1 ppb yr^{-1} in 2013-

https://doi.org/10.5194/acp-2020-481
Preprint. Discussion started: 29 July 2020


Atmospheric Chemistry and Physics Discussions

2016). It is unambiguous that the anomalously fluctuations of atmospheric CH_4 in this region are a warning to the world, its increasingly annual growth rate may be a dangerous signal to global climate change.

https://doi.org/10.5194/acp-2020-481
Preprint. Discussion started: 29 July 2020


Atmospheric Chemistry and Physics Discussions

1 Introduction

Since the pre-industrial era, the emissions of greenhouse gases (GHGs) have increased continuously, and larger absolute increases were found in recent years with the concentration higher than ever now (WMO, 2019). The GHGs could perturb the infrared radiation balance, trap the heat in the atmosphere, which contributes to global warming, melting glaciers, extreme weather events and many other global climate changes (IPCC, 2014). The recent 30-years from 1983 to 2012 were the warmest of the last 800-years in the Northern Hemisphere, and half of the rising surface temperature was due to increased GHGs emissions (IPCC, 2014). As one of the most important GHGs, the global warming effect of methane (CH_4) is just after carbon dioxide (CO_2) (Etminan et al., 2016). It has an 8-12 years atmospheric lifetime (Battle et al., 1996), with the global warming potential of ~23 times greater than CO_2 over a 100 year horizon (Weber et al., 2019). About 17% of radiative forcing by long-lived greenhouse gases was contributed by CH_4 during 1750-2016 (Etminan et al., 2016). Since the beginning of the industrial era, the concentration of CH_4 is rapidly increased because of the influence of anthropogenic activities (Saunois et al., 2016). The result by the analyses of ice cores in Antarctica showed that the atmospheric concentration of CH_4 has reached unprecedented over the last 0.8 million years (IPCC, 2014).

In the beginning of 1990s, CH_4 concentration appeared a decreasing trend in global scale. However, high growth rates were found in 1998, which was possibly due to the higher global mean temperature (Dlugokencky et al., 1998; Nisbet et al., 2014). Subsequently, a low growth rate sustained over 1999 to 2006, except for special years (2002/2003) with El Niño events (Dlugokencky et al., 1998). The annual growth rates dropped from ~12 ppb yr^{-1} to near 0 from late 1980s to 1999-2006 (Nisbet et al., 2019). But thereafter, the atmospheric CH_4 concentration keeps rising from 2007. During 2007-2013, the annual growth rate of methane was 5.7 ± 1.2 ppb yr^{-1}. After 2013, the atmospheric CH_4 grew even at rates not observed after 1980s, such as 12.7 ± 0.5 ppb yr^{-1} in 2014 and 10.1 ± 0.7 ppb yr^{-1} in 2015 (Nisbet et al., 2016, 2019). The overall

https://doi.org/10.5194/acp-2020-481
Preprint. Discussion started: 29 July 2020


Atmospheric Chemistry and Physics Discussions

77 global growth rate was 7.1 ppb yr^{-1} in recent 10 years (WMO, 2019). And the not
78 expected increase since 2007 would make it difficult to meet the targets of carbon
79 emission reduction in the future. The World Meteorological Organization/Global
80 Atmospheric Watch programme (WMO/GAW) annual greenhouse gas bulletin revealed
81 that globally averaged CH_4 mole fraction reached a new high with 1869 ± 2 ppb in 2018
82 (Rubino et al., 2019), which was ~259% of pre-industrial levels (~722 ppb around 1750
83 C.E.) (Etheridge et al., 1998; WMO, 2019).

84 The atmospheric CH_4 is mainly emitted from natural sources (about 40%, e.g.,
85 ruminants and wetlands) and anthropogenic sources (about 60%, e.g., paddies, cattle
86 ranch, coal mine, fossil fuel and biomass burning) (Hausmann et al., 2016; Saunois et
87 al., 2016). Studies from GAW observations indicated that the causes of recent increase
88 were likely attributed to anthropogenic emissions at mid-latitudes in the northern
89 hemisphere and the wetlands in the tropics (WMO, 2019). The rapid development of
90 population growth, economic expansion and countries urbanization has led to more and
91 more fossil fuel production and consumption (e.g., the large-scale exploitation of
92 natural gas, oil and coal) and biomass burning, consequently large amounts of
93 anthropogenic CH_4 were emitted around the world in recent years (Galloway, 1989;
94 Streets and Waldhoff, 2000; Wang et al., 2002; Lin et al., 2014; Hausmann et al., 2016).
95 The recent carbon isotope study revealed that biogenic emissions might also have
96 driven CH_4 increase, including microbial sources whether from rice, paddies,
97 ruminants, termites, enteric fermentation or all of these (Nisbet et al., 2016; Schaefer et
98 al., 2016; Wolf et al., 2017). 90% of CH_4 destruction in the atmosphere are mainly from
99 the reaction with hydroxyl radicals (OH) (Vaghjiani and Ravishankara, 1991; Bousquet
100 et al., 2011), an important oxidant in the troposphere (Logan et al., 1981). Therefore,
101 the interannual variability of OH or the decline oxidative capacity of the atmosphere
102 may also cause the recently increased CH_4 growth rates (Rigby et al., 2017; Turner et
103 al., 2017).

104 To get accurate understanding of atmospheric CH_4, a systematic observations

https://doi.org/10.5194/acp-2020-481
Preprint. Discussion started: 29 July 2020


Atmospheric Chemistry and Physics Discussions

network would perform the best. Hundreds of CH_4 observation stations worldwide are running under the framework of WMO/GAW. Since 1978, systematic measurements of atmospheric CH_4 began around the world (Blake et al., 1982; Rasmussen and Khalil, 1984; Dlugokencky et al., 1994). On the northern slope of the Mauna Loa volcano, Hawaii, there exists the first global station Mauna Loa (MLO), which was performed about 3397m above sea level (a.s.l.) and far away from local sources and sinks. It has the longest records of continuous atmospheric CH_4 observation (Keeling et al., 1976). Later, many types of the sites were installed CH_4 observation system, such as the Barrow (BRW), South Pole (polar site, SPO) (Dlugokencky et al., 1995), Cape Grim (CGO) in Australia (coastal/island sites) (Pearman and Beardsmore, 1984), Minamitorishima (MNM) in Japan (coastal/island sites) (Wada et al., 2007), Jungfraujoch (JFJ) in Switzerland and Mount Waliguan in China (continental mountain site) (Zhou et al., 2004; Loov et al., 2008). Even though, the exact causes of significantly increased CH_4 emissions in past years are still remained unclear and debated, especially for the anomalous periods with suddenly large growth, due to the time and space sparsity of measurements and the crude model approaches, which limited our understanding of the global variation of atmospheric CH_4 (Saunois et al., 2019; Weber et al., 2019). As long as the reasons for rising CH_4 emissions contributed by natural sources (e.g. wetlands), anthropogenic sources (e.g. fossil fuels), or climate change feedbacks remain uncertainties, it will be impractical to predict CH_4 trends in the future, and then to develop realistic management (Nisbet et al., 2019). Therefore, it is essential to establish typical observing regions and perform long observations.

China has the largest anthropogenic CH_4 emissions in the world (Janssens-Maenhout et al., 2019). Qinghai-Tibetan Plateau has an average altitude over 4000m a.s.l., which has long been recognized as the roof of the world. By coincidence, the two largest CH_4 source regions in the world (i.e. Eastern China and Northern India) trapped the Tibetan Plateau in the middle (Zhang et al., 2011; Fu et al., 2012; Wilson and Smith, 2015). Under the characteristics of special geographical conditions, lower population

https://doi.org/10.5194/acp-2020-481
Preprint. Discussion started: 29 July 2020


Atmospheric Chemistry and Physics Discussions

density, rarely industrial activities and high sensitivity to external disturbances, the Tibetan Plateau is undoubtedly one of ideal regions to observe continual CH_4 signal (Zhou et al., 2005; Fu et al., 2012; Zhang et al., 2013). Most of the previous studies reported the short-term CH_4 variations in China and concluded the importance of long-term observation (Cai et al., 2000; Zou et al., 2005; Wang et al., 2009; Fang et al., 2013), which is of great value to enhance the understanding of the global carbon cycle (Yuan et al., 2019). As the rapid development of China and India, the year to year difference as well as the sources and sinks of CH_4 on the Tibetan Plateau might change significantly over time. Since 1994, in-situ measurements of atmospheric CH_4 have been launched at Mt.Waliguan (WLG) station. To study the long-term variations of atmospheric CH_4 at the WLG and get a new insight of its characteristics in the inland of the Eurasia, in this study, we evaluated the performance of a 24 year long-term in situ observations of CH_4 at Mt.Waliguan baseline observatory, which is the longest time observing records in China. Temporal patterns, annual variations, long-term trends, air mass transports, spatial distribution of potential sources were analyzed. In addition, the case studies combining atmospheric CO measurements and a separate analysis between the Tibetan Plateau and the city regions were performed to constrain the contribution of anthropogenic emissions.

2 Methodology

2.1 Measurement site

The Mt.Waliguan (WLG, 36.28° N, 100.09° E, 3816m a.s.l.) station is situated at the edge of northeastern of the Tibetan (Qinghai-Xizang) Plateau, which was in remote western China and isolated from populated and industrial regions (Fig. 1). WLG was the only WMO/GAW global background station in Eurasia and running by the China Meteorological Administration (CMA). The surrounding areas of the site are pristine with sparse vegetation, naturally arid and semi-arid grasslands. Small farms with yak

https://doi.org/10.5194/acp-2020-481
Preprint. Discussion started: 29 July 2020


Atmospheric Chemistry and Physics Discussions

and sheep are in the valley. Two adjacent large cities Xining (~2.2 million populations) and Lanzhou are located about 90km northeast and 260km east of the station, respectively. The Longyangxia hydroelectric station (~380 km^2) is located approximately 13km south to southwest of the WLG. The predominant winds at WLG are mainly from southwest and east in winter and summer, respectively (Zhou et al., 2004; Zhang et al., 2011), which is controlled by Tibet Plateau monsoon. Simultaneously, dial variations of vertical winds at WLG is influenced by mountain-valley breezes, where upslope flow brings heated air masses from the boundary layer to the site in daytime and downslope flow results in cool air masses transport from mountain peak to the site. Under this unique location, the observation at WLG could obtain essential information on CH_4 sources and sinks from Eurasia (Zhou et al., 2005; Zhang et al., 2013).

2.2 Instrumental setup

Atmospheric CH_4 has been measured quasi-continuously using a HP 5890 gas chromatograph (GC) equipped with a flame ionization detector (FID) since July 1994, and an Agilent 6890N GC equipped with a FID since June 2008. Both of the systems used the same sampling procedures. A Cavity Ring Down Spectroscopy system (Picarro G1301) began in January 2009 and the instrument was upgraded to Picarro G2401 in 2015. Ambient air is delivered to the above systems at about 5 L/min by a KNF Neuberger N2202 vacuum pump via a dedicated 0.95 cm o.d. sample line from an 80m intake line attached to an 89m steel triangular tower located approximately 15m from the main observatory. The residence time of the ambient air from the top of the tower to the instrument is 30 s. The ambient air is first passed through a 7 mm stainless steel membrane filter located upstream of the pump and then (after the pump) passed through a pressure relief valve set at 1 atm to release excess air and pressure. The ambient air is then dried to a dew point of approximately -60°C by passing it through a glass trap submerged in a -70°C methanol bath. All standard gases supplied to the instruments are

https://doi.org/10.5194/acp-2020-481
Preprint. Discussion started: 29 July 2020


Atmospheric Chemistry and Physics Discussions

from pressurized 37.5 L treated aluminum alloy cylinders fitted with high-purity, two-stage gas regulators. Stainless steel tubing (0.32 cm o.d., 0.22 cm i.d.) is used for the standard gas sample line and the ambient sample line after the cold trap. The automated sampling module equipped with a VICI 8 ports valve is designed to sample from separate gas streams (standard tanks and ambient air). According to the comparability target of WMO/GAW program (WMO, 2019), methane mole fractions are referenced to a Working High standard (WH) and a Working Low standard (WL). Additionally, a calibrated cylinder filled with compressed ambient air is used as a Target gas (T) to check the precision and stability of the system routinely. Diagram of the observing system during different periods could be seen at Zhou et al. (2004) and Fang et al. (2013). Here, we focus on the longest continuous measurements of CH_4 from August 1994 to May 2017 at WLG. Data gaps in limited periods are because of the malfunction of instrument and the maintenance of the sampling system.

The records of CO in this study was initinially observed by an RGA-3 gas chromatograph (GC) equiped with an HgO reduction detector (Trace Analytical Inc.) since 1994. An automated sampling module was designed to sample from ambient air and a series 9 standards. Deailed diagram of the system was described by Zhang et al. (2011). Since 2010, the CO has been measured by the Cavity Ring Down Spectroscopy instrument (Picarro G1302 and G2401 since 2015). The scale for all of the CO measurement were further updated to WMO X2014A.

2. 3 Data processing

Most on-site CH_4 observations were unavoidably influenced by local sources and other complex conditions (e.g., traffic transportation, various topography). As a result, the records cannot fully represent the regional atmospheric CH_4 in well-mixed conditions (Liu et al., 2019). To precisely get representative regional records, we exclude CH_4 measurements influenced by local sources adjacent to the site (e.g., agricultural fields, cities, traffic emissions). The hourly CH_4 data were classified as Local/Regional events

https://doi.org/10.5194/acp-2020-481
Preprint. Discussion started: 29 July 2020


Atmospheric Chemistry and Physics Discussions

through the meteorological approach, which was based on essential meteorological information, similar to previous studies by Zhou et al. (2004) and Liu et al. (2019). In this study, the CH_4 records associated with surface wind from selected sectors (i.e. NNE-…-ENE in spring, NE-…-SE in summer, NE-…-ESE in autumn, and NE-ENE in winter) were flagged as local representative. Subsequently, we further rejected portion of daytime records to minimize the effect of human activities (e.g., rush hours), including 9:00-13:00 LT (local time) in spring and summer, 9:00-14:00 LT in autumn, 10:00-17:00 LT in winter. Finally, we filtered CH_4 data into local events when the surface wind speed was less than 1.5 m s^{-1} to minimize the very local accumulation.

To understand the influence of local surface wind, the hourly CH_4 data was calculated versus 16 horizontal wind directions (Fang et al., 2013). In this study, we used the 'polarPlot' function located in the 'openair' package of the statistical software R (R Core Team, 2020). It shows the bivariate (i.e. wind speed and wind direction) polar plot of CH_4 concentrations, and the concentrations are calculated as a continuous surface by modelling using smoothing techniques (Carslaw et al., 2006; Diederich, 2007). Also, conditional probability function (CPF) was used to detect the probability of which wind directions are dominated by high CH_4 mole fractions (Uria-Tellaetxe and Carslaw, 2014). In order to study the pollution transport pathways of air masses at WLG, the cluster analysis of 3 days back trajectories was applied using the Hybrid Single-Particle Lagrangian Integrated Trajectory (HYSPLIT) dispersion model (Draxier and Hess, 1998; Rousseau et al., 2004) on the strength of gridded meteorological data (2004-2017) from the National Oceanographic and Atmospheric Administration's Air Resources Laboratory (NOAA-ARL). The trajectories in four months, including January, April, July and October, were calculated to represent the seasons of winter, spring, summer and autumn, respectively. The spatial source distributions of annual CH_4 were analyzed using the Potential Source Contribution Function (PSCF) approach, which computed the conditional probability of the residence times of air parcels with greater concentration than threshold transport to the

https://doi.org/10.5194/acp-2020-481
Preprint. Discussion started: 29 July 2020

Atmospheric Chemistry and Physics Discussions

exactly receptor site (Ashbaugh et al., 1985). In this study, PSCF value was calculated in 0.5×0.5-degree grid cell (i, j):

$$\mathrm{PSCF}_{ij} = m_{ij} / n_{ij} \quad (1)$$

n_{ij} represents the number of endpoints that terminate in the ijth grid cell, while the number of trajectories with concentration exceed the threshold value was defined as m_{ij} (Polissar et al., 1999). In order to reduce the abnormal influence of small n_{ij} values in some grid cells, PSCF_{ij} was further computed by an arbitrary weighting function W_{ij} as below.

$$W_{ij} = \begin{cases} 1.00 & 3n_{ave} < n_{ij} \\ 0.70 & 1.5n_{ave} < n_{ij} \le 3n_{ave} \\ 0.42 & n_{ave} < n_{ij} \le 1.5n_{ave} \\ 0.05 & n_{ij} \le n_{ave} \end{cases} \quad (2)$$

W_{ij} represents the weight of cell (i, j), n_{ij} is the number of trajectory endpoints that fall in the ijth grid cell, while the n_{ave} shows the mean number of the endpoints in all grid cells.

In order to fill the data gaps so as to evaluate the long-term CH_4 trend, we applied the curve fitting approach by Thoning et al. (1989). We also calculated the trend curve that excluded the influence of seasonal variation, and then got the annual growth rates of the average of the first derivative of the trend curve. The function consists of the polynomial part and the annual harmonics part:

$$f(t) = a_0 + a_1 t + a_2 t^2 + \cdots + a_{(k-1)} t^{(k-1)} + \sum_{n=1}^{nh} c_n [\sin(2n\,\pi\,t) + \varphi_n] \quad (3)$$

'k' represents the number of polynomial part. 'nh' is the number of harmonics part. We applied k = 3 polynomial terms (a quadratic) for multi-year trends and nh = 4 yearly harmonics for seasonal cycles in this study. The fast Fourier transform (FFT) was utilized to smooth the fitting residuals (Press et al., 1992).

The significant difference test was applied by the 'scheirerRayHare' function in the 'rcompanion' package of R software, which is a non-parametric test for two-way ANOVA analysis. And the multiple comparison was used by Wilcoxon rank sum test

https://doi.org/10.5194/acp-2020-481
Preprint. Discussion started: 29 July 2020

Atmospheric Chemistry and Physics Discussions

with R (R Core Team, 2020). For the correlation analysis between CH_4 and CO, we obtained the detrended time series of CH_4 and CO from 2004-2017 based on the method by Thoning et al. (1989). The detrended values are denoted as ΔCH_4 and ΔCO. To obtain the correlation slopes of ΔCH_4 and ΔCO accurately, a rolling linear regression was applied to ΔCH_4 and ΔCO time series by the 'roll_lm' function in 'roll' package of R (R Core Team, 2020). We successively moved a 24-h time window by 1 h over the whole time series. Similar to the study by Tohjima et al. (2014), we set 3 criteria to achieve a better quality control of the slopes. When (i) the number of CH_4 record is less than 5 in 24 hours, (ii) the coefficient variation of the correlation slope is more than 15%, (iii) the absolute value of the correlation slope is less than 0.8 ($|R| < 0.8$), the correlation slopes were identified as statistically insignificant and inaccurately and were rejected. In order to understand the year to year variations, we further analyzed the different periods over 1994-2017. The entire CH_4 time series were divided according to the significant stages or the critical time period of atmospheric CH_4 variations from previously studies (Zhou et al., 2004; Fang et al., 2013; Zhang et al., 2013; Nisbet et al., 2019; WMO, 2020), appropriately every five years a period. Unless special notes, the average values in this study were presented with 95% confidence intervals (CIs).

3 Results

3.1 Diurnal variations

Generally, distinct diurnal cycles were observed in four seasons during 1994-2017. The CH_4 mole fraction increased from early morning and reached the maximum at noon and a trough in late afternoon (Fig. 2f). However, differences also existed from different seasons. In spring, the atmospheric CH_4 apparently increased from 9:00 to 13:00 LT with the daily amplitude of 5.7 ±2.4 ppb. In summer, the elevated CH_4 also appeared during 9:00-13:00 LT at noon, and the daily amplitude was 4.3 ± 2.6 ppb. In autumn, the diurnal variation showed the mean amplitude of 4.5 ±2.4 ppb, significantly elevated

https://doi.org/10.5194/acp-2020-481
Preprint. Discussion started: 29 July 2020


Atmospheric Chemistry and Physics Discussions

296 CH_4 reached at 9:00-13:00 LT with one peak at noon. In winter, largely increasing
297 presented in the daytime at 9:00-17:00 LT, with the largest amplitude of 6.2 ± 2.4 ppb
298 among four seasons. For the diurnal variation over the whole monitoring period, the
299 highest CH_4 mole fraction was observed in winter and the minimum value was found
300 in spring (Fig. 2f).

301 Different patterns for diurnal CH_4 cycles were also found over different periods.
302 In 1994-1997 and 1998-2002, the CH_4 mole fractions in winter were apparently higher
303 than the other seasons (Fig. 2a-b). But its value was the highest in summer during the
304 period of 2003-2007, 2008-2012 and 2013-2017 (Fig. 2c-e). The atmospheric CH_4
305 values in winter were gradually falling behind the other seasons, and the gaps among
306 different seasons were increasing, especially for summer. Before 2002, diurnal cycles
307 in four seasons were ambiguous (Fig. 2a-b), but significant diurnal variations appeared
308 afterwards (Fig. 2c-e). The peak to trough amplitude almost increased along with the
309 time in almost all seasons. For example in spring, the amplitude was 6.5 ± 3.0, 4.7 ±
310 1.8, 5.6 ± 2.6, 6.2 ± 2.4 and 6.8 ± 3.4 ppb over 1994-1997, 1998-2002, 2003-2007,
311 2008-2012 and 2013-2017, respectively (Table S1).
312

313 **3. 2 The impact of local surface winds**

314 As observed by the previous short-term variations, the atmospheric CH_4 at WLG was
315 significantly influenced by local surface wind from northeast to southeast sectors (Fig.
316 3f). Slight differences were also found among seasons. In spring, the atmospheric CH_4
317 was enhanced by 2.5-6.5 ppb compared to the seasonal average (1839.7 ± 1.4 ppb)
318 when the wind was originating from NNE-NE-ENE-E sectors. In summer and autumn,
319 the wind from NNE-NE-ENE-E-ESE induced higher CH_4 mole fractions, with
320 enhancement of about 3-9.5 ppb and 4 to 18 ppb, respectively. In winter, the CH_4 mole
321 fractions significantly elevated from the wind sectors that same as those found in spring,
322 with value of 7-21 ppb than seasonal average (1854.5 ± 4.8 ppb). Relatively, the
323 amplitude of enhancements in winter and autumn were larger than those in spring and

https://doi.org/10.5194/acp-2020-481
Preprint. Discussion started: 29 July 2020


Atmospheric Chemistry and Physics Discussions

summer.

What interesting is that wind sectors elevating CH_4 mole fractions vary in different periods. The early periods (i.e. 1994-1997 and 1998-2002) were different from the recent periods (2003-2007, 2008-2012 and 2013-2017). The elevated CH_4 was predominately from about ENE-E-ESE-SE-SSE sectors in early years (Fig. 3a-b), but evolved to NNE-NE-ENE-E sectors in later years (Fig. 3c-e). Furthermore, the amplitude of enhancements was almost increasing continuously along with the time. For example, in autumn, the maximum CH_4 mole fractions were from E, ENE, ENE, NE and ENE sectors in 1994-1997, 1998-2002, 2003-2007, 2008-2012 and 2013-2017, with the successively increasing enhancements of 8.6, 12.1, 14.7, 16.8 and 19.7 ppb, respectively.

We applied the CPF to hourly CH_4 and CO data by considering intervals of entire data percentiles including 0-20, 20-40, 40-60, 60-80 and 80-100 to draw the CPF polar plot. It is clear that different sources only affected CH_4 mole fractions on different percentile range. For example, for most wind speed-directions the CPF probability of CH_4 being greater than the 60^{th} percentile was tending to zero (Fig. 4). And it is apparent that most sources contributed to the less than 60^{th} percentiles of CH_4 mole fraction (e.g. 40-60) (Fig. 4). The specific sources were prominent for specific percentile ranges. The wind from the southwest and southeast was important on the cases of the higher percentiles, resulted in the highest CH_4 mole fractions of 1849-1872 ppb for 60-80 percentile and 1872-2031 ppb for 80-100 percentile (Fig. 4). It's more obvious that the CO showed gradually shifted sources with the increase of percentile ranges. The areas where the CPF probabilities were higher is to the NW-SW sectors when the percentages ranged from 0 to 40^{th}. Nevertheless, when the percentages were larger than 60^{th}, the high probability areas completely moved to NE-SE sectors (Fig. 4).

https://doi.org/10.5194/acp-2020-481
Preprint. Discussion started: 29 July 2020


Atmospheric Chemistry and Physics Discussions

3.3 Air mass pathways and potential source distributions

3.3.1 Air mass transports

Figure 5 illustrates the cluster analysis to the 3-day back trajectories to WLG during 2004-2017. In spring, the majority of the air masses were from west and northwest regions, which accounted for about 24% (cluster 3) and 44% (cluster 5) of total trajectories (Fig. 5a). These air masses were also accompanied with higher CH_4 mole fractions than those from east and northeast regions, i.e. cluster 1 (13.3% of total) and cluster 4 (11.69%) (Table 1). The largest enhancement was ~18 ppb (relative to spring average) by cluster 3. In summer, 45% of air masses (cluster 1) were from eastern regions. But the high CH_4 mole fractions were on cluster 2 and cluster 5 from northwest and west regions, although low percentages were found (cluster 2: 26%; cluster 5: 7%) (Fig. 5b). The highest CH_4 mole fraction was associated with cluster 2, with ~9 ppb larger than the average in summer. In autumn, large proportion of air masses was originating from west and southwest station, such as cluster 2 (49%) and cluster 3 (32%) (Fig. 5c). The highest CH_4 was from cluster 3 with enhancement of ~4 ppb than the seasonal average. Similar to autumn, the air masses were primarily from northwest in winter, including northwest cluster 3 (59%) and southwest cluster 1 (34%) regions (Fig. 5d). The highest CH_4 mole fractions was on cluster 1with the enhancement of ~7 ppb than the average value.

3.3.2 Spatial distribution of potential source regions

In this study, the potential sources were analyzed over different periods, i.e. 2004-2007, 2008-2012 and 2013-2017. Generally, the strong potential sources were located at the northeast to southeast of the station, especially in summer, but the source regions differed in various seasons as well as years (Fig. 6). The regions of potential source in spring (Fig. 6a-c) and winter (Fig. 6j-l) was obviously larger than that in summer (Fig.

https://doi.org/10.5194/acp-2020-481
Preprint. Discussion started: 29 July 2020


Atmospheric Chemistry and Physics Discussions

6d-f) and autumn (Fig. 6g-i). There were also trends for the CH_4 source regions along with years: i) the area of potential source regions was increasing with the years, and ii) the location of strong potential sources changed along with the time. For example in autumn and winter, the strength of CH_4 sources were very strong in the southeast to northeast during 2004-2007 (Fig. 6g & i), and then weaked in 2008-2012 (Fig. 6h & k), and finally (i.e. 2013-2017), almost vanished in eastern regions but moved to southwest with very large distribution area (Fig. 6i & l).

3.4 Extracting the well-mixed ambient methane

To precisely understand characteristics of atmospheric CH_4, e.g., seasonal cycle or long-term trend, it is vital to identify the CH_4 records that were influenced by local sources and sinks. In this study, we analyzed hourly CH_4 measurements during 1994-2017, and 47.3% of CH_4 data were classified as regional representative, with the average CH_4 mole fraction of 1847.9 ± 0.3 ppb. The local representative data was obviously larger than regional events, with an average value of 1858.2 ± 0.4 ppb (Table 2). The proportion of regional events increased slightly before 2012, but significantly reduced in recent years (e.g., 2013-2017). The filtered regional/local time series was shown in Figure 7. It can be seen that the CH_4 mole fractions obviously increased from 1994 to 2017. The atmospheric CH_4 showed strong growth and displayed large fluctuation at WLG (Fig. 7). In 1995, the average CH_4 mole fraction was only 1805.8 ± 0.1 ppb, however, the average value increased 98 ppb by the year of 2016 (1903.8 ± 0.1 ppb) (Table 3).

3.5 Correlation analysis between CH_4 and CO

Because part of CH_4 and CO in atmosphere are from the same anthropogenic sources (e.g., fossil fuel combustion), we calculated the regression slopes of $\Delta CO/\Delta CH_4$ from 2004 to 2017 (Fig. S1). Figure 8 presents the average seasonal cycles of the $\Delta CO/\Delta CH_4$

https://doi.org/10.5194/acp-2020-481
Preprint. Discussion started: 29 July 2020


Atmospheric Chemistry and Physics Discussions

slopes. Generally, the slopes were larger in summer and lower in winter during the observing period, except for 2004-2007 with the high slope in autumn. Additionally, the regression slopes increased along with the time, which showed the maximum in 2013-2017 and the minimum in 2004-2007. For the year to year variations, the $\Delta CO/\Delta CH_4$ slopes showed large fluctuations from 2004 to 2017 at WLG (Fig. 9). The slopes showed decreasing trend during 2004-2007 but then increased from 2007 to 2010, and again decreased after 2010. In spring and summer, increasing trends appeared again after 2014. The slopes in summer were almost the largest but the lowest in winter.

3.6 Variation of long-term records

3.6.1 Seasonal cycles

In order to further investigate the characteristics of atmospheric CH_4, we divided the CH_4 observations into two main regions according to the above analysis, including geographical conditions, the effect of surface winds, the long-range transports and the potential source distributions. The first region was covered the northeast to southeast (NNE-…SE) of WLG, which was denoted as City Regions (CR). The second region was located south to west (S-…-W) of the station and was well known Tibet (Qinghai-Xizang) Plateau (TP) (Fig. S2). Accordingly, the hourly CH_4 records when the surface wind coming from these sectors were divided into two subsets (i.e. TP and CR). The long-term variations between the two regions as well as the total regional time series (Total) were compared and analyzed to explore new sight of atmospheric CH_4 variation at WLG.

Overall, at WLG, the seasonal averages of CH_4 were ordered by summer (1850.0 ± 0.3 ppb), winter (1847.4 ± 0.3 ppb), autumn (1844.4 ± 0.3 ppb) and spring (1841.2 ± 0.3 ppb), except during 1994-1997 with the maximum in winter and minimum in autumn (Fig. 10). Seasonal averages in CR were significantly different to that in TP and also the entire regional data (Total). The seasonal average in TP was mostly higher than

https://doi.org/10.5194/acp-2020-481
Preprint. Discussion started: 29 July 2020


Atmospheric Chemistry and Physics Discussions

that in CR, except for wintertime (Table S2). The atmospheric CH_4 in August was mostly the maximum and the April was the minimum for the total regional time series (Total), with the seasonal amplitude of 13.4 ppb. The peak to trough amplitude in CR (~15 ppb) was higher than that in TP (~13 ppb) during 1994-2016. Additionally, seasonal amplitudes indicated different trends between CR and TP. For CR, the seasonal amplitude was firstly dropped and then increased along with time, which were similar to the variation of total regional events (Total). But for TP, the amplitude displayed a continuously increasing trend, with values of about 15.9, 19.3, 21.6, 23.4 and 22.4 ppb in 1994-1997, 1998-2002, 2003-2007, 2008-2012 and 2013-2016, respectively.

3.6.2 Long-term trend

In the 1990s, the CH_4 growth rates were very low and even negative at WLG. Subsequently, during 2002-2006, a steady period was found with a near-zero growth rates. After 2007, the atmospheric CH_4 was raised significantly (Fig. 11a). In the year of 1997/1998, 2000/2001, 2007/2008 and 2011/2012, larger amplitude of the growth rates was found and strong growth appeared (Fig. 11b). The growth rates fluctuated evenly with both positive and negative values before 2009. But almost all of the growth rates showed a positive value after 2009. From 1990s to 2010s, three apparently developing stages (i.e. highlighted green, blue and red blocks) were presented, the CH_4 mole fraction slightly decreased in 1998-2000 (green color), and then go through a relative steady period in 2003-2006 (blue color), finally increased steadily after 2007 (red color) (Fig. 11).

The overall annual growth rates were 5.1 ± 0.1 ppb yr^{-1} over 1994-2016 at WLG (Table 4). However, the periodic annual growth rats were 4.6 ± 0.1, 2.6 ± 0.2, 5.3 ± 0.2, 7.6 ± 0.2 and 5.7 ± 0.1 ppb yr^{-1} in 1994-1997, 1998-2002, 2003-2007, 2008-2012 and 2013-2016, respectively. The CH_4 growth rate in CR was significantly different from that in TP (Fig. S3). In 1994-1997, 2003-2007 and 2013-2016, the growth rates in TP were obviously larger than that in CR (Table 4). But in 2003-2007 and 2008-2012, the

https://doi.org/10.5194/acp-2020-481
Preprint. Discussion started: 29 July 2020


Atmospheric Chemistry and Physics Discussions

458 CR showed higher annual growth rates. In addition, for the entire observing period (i.e.
459 1994-2016), the growth rates in both TP (5.2 ± 0.1 ppb yr^{-1}) and CR (5.0 ± 0.1 ppb yr^{-1})
460 were similar to the overall annual growth rates (Fig. S3).
461
462 **3. 7 Case study for air mass transport**

463 As described above, the northeast and southeast city regions might act as strong
464 regional sources influencing the atmospheric CH_4 at WLG. Therefore, to analyze the
465 effect of long-distance transport of emissions from cities, we further excluded the
466 regional data by air mass transport, and the rest of regional records were denoted as
467 'TR'. We applied the monthly cluster analysis to hourly trajectories over 2005-2007,
468 2008-2012 and 2013-2017. The cluster results from city regions were presented in detail
469 in Fig. S4 and Table S3.
470 The proportion of trajectories from cities was 40.3%, 32.5% and 6.8% in 2005-
471 2007, 2008-2012 and 2013-2017, respectively. And about 22.8%, 35.6% and 38.4% of
472 the regional records were associated with air masses transport from city regions in
473 2005-2007, 2008-2012 and 2013-2017, respectively (Table 5). The average CH_4 value
474 when air masses transport from city regions (1863.0 ± 0.3 ppb) was obviously higher
475 than other sectors (1850.6 ± 0.2 ppb) (Fig. S5). However, after excluding the CH_4
476 records when air trajectories transport from city regions, the growth rates of TR in 2008-
477 2012 (10.1 ± 0.1 ppb yr^{-1}) and 2013-2017 (6.3 ± 0.1 ppb yr^{-1}) (Table 5) were higher
478 than the original regional data series (i.e. 7.6 ± 0.2 and 5.7 ± 0.1 ppb yr^{-1}) (Table 4).
479 And the overall growth rate for TR in 2005-2016 or 1994-2016 was still similar to
480 original data series (Total), no significant difference was found (Fig. S5).
481

https://doi.org/10.5194/acp-2020-481
Preprint. Discussion started: 29 July 2020


Atmospheric Chemistry and Physics Discussions

4 Discussion

4. 1 Anthropogenic emission on temporal patterns

In the early years, the daily cycles of atmospheric CH_4 at WLG were not distinct and the amplitude was small (Fig. 2a-b), which were similar to the previous studies by Zhang et al. (2013) and Fang et al. (2013). The ambiguous diurnal patterns indicated that the local sources were weak at WLG in the past. The apparent diurnal cycles after 2000 may be attributed to the intense activities by human (e.g., grazing, fuel burning), which was aggravated in daytime and weak in nighttime (Fang et al., 2013). The meteorological conditions (e.g., diffusion and transport) could contribute to the increasing CH_4 amplitudes. The WLG was remote from the populate center, the good diffusion condition in daytime may bring high CH_4 mole fractions to the site. The increasing amplitude (Table S1) and CH_4 mole fractions over time suggested that the WLG was affected by increasingly local sources (e.g., human activities) (Zhou et al., 2004). The maximum was found in summer in recent years (Fig. 2e) could also be ascribed to the transport of anthropogenic sources by the meteorological factors. In summer, the intensely herd or graze activities around WLG might enhance the regional CH_4 emissions and hence contribute to the higher CH_4 mole fractions. The higher CH_4 mole fraction in winter in past years (Fig. 2a) was probably because of the way of heating (e.g., large biomass burning) as well as the adverse diffusion conditions in cold weather.

The previous study by Zhou et al. (2004) found that higher CH_4 mole fractions appeared when the winds come from the ENE-E-ESE-SE sectors at WLG during 1991-2002, which was similar to our study in similar period (Fig. 3a-b). Causes of the elevated CH_4 from these wind sectors could be attributed to the large plantation of highland barley as well as high population density in those areas (Fang et al., 2013). Two largest cities Xining and Lanzhou are situated in northeast and east of WLG, respectively, which could emit large amount of CH_4 by human activities. Besides,

https://doi.org/10.5194/acp-2020-481
Preprint. Discussion started: 29 July 2020


Atmospheric Chemistry and Physics Discussions

509 previous studies on black carbon (BC) and carbon monoxide (CO) indicated that the
510 emissions from the Yellow River Canyon industrial area, ~500km away from northeast
511 of WLG may also donate to the high CH_4 values originating from ENE and NE sectors
512 (Zhou et al., 2003). In summer, the prevailing wind directions were from NE-…-ESE
513 sectors (~46%) (Fig. S6), and the CH_4 mole fractions were also higher in the related
514 sectors. However, in the autumn and winter, although the prevailing wind and high wind
515 speed were from SSW-…-W sectors (~ 40-50%) (Fig. S6), the high CH_4 mole fractions
516 were from almost the opposite wind sectors of NNE-….-ESE (Fig. 3f), which indicated
517 that strong local sources were distributed from northeast to southeast (city regions), and
518 even covered the emissions of natural sources. As time goes on, the wind sectors with
519 high CH_4 mole fractions changed and concentrated on ESE to ENE sectors, and the
520 amplitudes of enhancements were increasing, which further implied the effect of
521 stronger emissions from anthropogenic sources in city regions in recent years.
522

523 **4. 2 Pollutant sources regions**

524 **4. 2. 1 Sources regions**

525 The air masses from east and northeast regions passed over the cities of Xining and
526 Lanzhou (capital of Gansu province), which is the populated center and industrial area
527 (Fig. 5). However, the highest CH_4 values was not observed when air mass was from
528 these sectors. Instead, high CH_4 mole fractions were frequently observed when air mass
529 from the northwest to southwest (Table 1). It was possibly due to that the air masses
530 from west and northwest had passed through the northwest of Qinghai province and the
531 central area of Xinjiang Uygur Autonomous Region (XUAR), where located Ge'ermu
532 urban area (the second largest city of Qinghai) with rapid industrial development,
533 natural gas and petroleum resources exploitation and large crops residue burning
534 (Zhang et al., 2013). Similar to the CPF percentile analysis (Fig. 4), the southwest or
535 northwest region away from the site may be also strong source regions.

https://doi.org/10.5194/acp-2020-481
Preprint. Discussion started: 29 July 2020


Atmospheric Chemistry and Physics Discussions

536 Most potential source identified in northwestern regions (Fig. 6) was possibly due
537 to CH_4 emissions from the northwest Gansu province, the northwest Qinghai province
538 and the southeast of XUAR. The different source distribution by seasons could be
539 attributed to the effect of westerlies or the southeast monsoons (Zhou et al., 2004). The
540 obviously increasing source region was clear evidence for the strong effect of the
541 expansion of human activity. Moreover, the pattern of source region moved from the
542 east to the southwest, especially in autumn and winter, indicated that the southwest
543 away from the WLG, e.g., Northern India, were gradually becoming a strong CH_4
544 source region. India has abundant cattle as well as extensive large-scale coal mining,
545 large amount of CH_4 emissions may transport from northern India to the northeastern
546 Tibetan Plateau (Fig. 6i & l). The air mass transport result (Fig. 5d) also support the
547 result that the southwest air masses (cluster 1) contributed the highest CH_4 mole
548 fractions. The studies of atmospheric Hg at WLG by Fu et al. (2012) also revealed this
549 phenomenon.
550
551 **4. 2. 2 Different sources between CH_4 and CO**

552 The percentile polar plot clearly showed the specific distribution of different CH_4 mole
553 fractions (Fig. 4). The result revealed that most areas around WLG contributed to low
554 CH_4 mole fractions, the southeast and southwest of the site exist two strong source
555 regions. It is of great possible that the anthropogenic emission from cities (e.g.,
556 Lanzhou, Chengdu, etc.) was the only cause for high values in the southeast, and the
557 southwest region away from WLG was possibly due to sources from other countries,
558 such as India. Unlikely to the CH_4, the high CO mole fractions were consistent from
559 east regions (urbanized area) (Fig. 4), indicating strong anthropogenic sources in city
560 regions (i.e. Xining and Lanzhou) (Zhang et al., 2011).
561 The seasonal cycles of $\Delta CO/\Delta CH_4$ slopes (high in summer and low in winter) (Fig.
562 8) may primarily be due to the effect of monsoons and air mass transport. In summer,
563 air masses arriving at WLG were predominantly transported from the northeast to east

https://doi.org/10.5194/acp-2020-481
Preprint. Discussion started: 29 July 2020


Atmospheric Chemistry and Physics Discussions

564 city regions (e.g., Xining, Lanzhou) with the largest CO mole fractions. In contrast, the
565 air masses were mainly from the southwest in winter, which carried strong CH_4
566 emissions but few CO emissions (Zhang et al., 2011) (Table 1). Hence the opposite two
567 air mass transport lead to a peak in summer and a trough in winter (Fig. 8). Moreover,
568 we could see apparently regional polarization in the concentration ratio of CH_4 and CO
569 (Fig. S7), implying the different strong source distribution between CH_4 and CO at
570 WLG. The cluster results (Fig. 5b & d) and the potential sources analysis (Fig. 6f & l)
571 also support this seasonal variation. Tohjima et al. (2014) found an opposite variation
572 at Hateruma Island, which showed low slope values in summer. It could be attributed
573 to different local sources and sinks, suggested the special topography condition and
574 local source distribution around WLG. The large $\Delta CO/\Delta CH_4$ fluctuations (Fig. 9) over
575 the study period was likely because of the anomaly years of different CH_4 or CO mole
576 fractions as well as source regions. In 2007, large increase of ΔCH_4 appeared, and from
577 2010 to 2013, the ΔCO decreased significantly (Fig. S1). Before 2010, large air masses
578 and potential source regions were identified in eastern regions (city regions) with the
579 highest CO emission (Fig. 5; Fig. 6). After 2010, the southwest regions showed high
580 contributions, with the highest CH_4 emission but relatively lower CO emission.
581 Therefore, obviously variation of the slopes presented with almost an increase in 2007-
582 2010 and a decrease after 2010 (Fig. 9).
583

584 **4. 3 Long-term variations**

585 **4. 3. 1 Seasonal cycles**

586 The seasonal variations with maximum in summer and minimum in spring at WLG
587 (Fig. 10) were consistent with the previously short-term studies, e.g., Zhang et al.
588 (2013) in 2002-2006. However, it was almost opposite to observation in the adjacent
589 stations such as Lin'an, Shangdianzi and Longfengshan in China (Fang et al., 2013,
590 2016), as well as most global stations in the northern hemisphere, e.g., MLO, BRW and

https://doi.org/10.5194/acp-2020-481
Preprint. Discussion started: 29 July 2020


Atmospheric Chemistry and Physics Discussions

591 JFJ (Dlugokencky et al., 1995; Loov et al., 2008). We further compared similar
592 WMO/GAW global stations in the north hemisphere, including MLO (19.54° N, -
593 155.58° E, 3397m a.s.l.) (Dlugokencky et al., 1995, 2019a), JFJ (46.55° N, 7.99° E,
594 3580m a.s.l.) (Zellweger et al., 2016), MNM (24.29° N, 153.98° E, 7.1m a.s.l.)
595 (Matsueda et al., 2004; Tsutsumi et al., 2006), as well as the marine boundary layer
596 (MBL) from NOAA/ESRL lab at similar latitude (Dlugokencky et al., 2019b). It can be
597 seen that the stations in the northern hemisphere (i.e. MLO, JFJ and MNM) and the
598 MBL showed an opposite trend to WLG with the minimum in summer and maximum
599 in winter or spring (Fig. 12). And the seasonal amplitude at WLG (~14 ppb) was lower
600 than many other sites in the northern hemisphere, about 35-70 ppb, e.g., MLO, BRW,
601 bialystok in Poland, ochsenkopf in Germany and beromunster in switzerland
602 (Dlugokencky et al., 1995; Thompson et al., 2009; Popa et al., 2010; Satar et al., 2016).
603 MBL also showed larger amplitude than that in WLG (Fig. 12). The low amplitude at
604 WLG was possibly because of high elevation of continental mountain sites (e.g., WLG,
605 JFJ), where were relatively less affected by local influences than the coastal/island sites
606 (Yuan et al., 2019). The peak in summer at WLG may be attributed to larger grazing
607 and human activities than other seasons. The CH_4 emissions from yaks and other
608 ruminants in Tibetan Plateau (alpine pasture) were very strong in summer, preceded
609 only by paddy emission (Fang et al., 2013; Zhang et al., 2013). Furthermore, the
610 photochemical capacities were very weak (high altitude) and the dynamic transport by
611 air flow from polluted northeast/southeast region was also strong in summer at WLG,
612 which all induced high CH_4 mole fractions in summer and consequently an opposite
613 trend with other sites (Ma et al., 2002; Xiong et al., 2009).
614
615 **4. 3. 2 Long-term trends in different observing periods**

616 The entirely fluctuant trend of atmospheric CH_4 in 1994-2016 at WLG (Fig. 11) was
617 similar to the global trend reported by quite a few studies (Bergamaschi et al., 2013;
618 Rigby et al., 2017; Nisbet et al., 2019). The previous study by Zhou et al. (2004) showed

https://doi.org/10.5194/acp-2020-481
Preprint. Discussion started: 29 July 2020


Atmospheric Chemistry and Physics Discussions

619 the CH_4 annual increase of 4.5 ppb yr^{-1} in 1992-2001, which was similar to that in 1994-
620 1997 (4.6 ± 0.1 ppb yr^{-1}) and 1997-2002 (2.6 ± 0.2 ppb yr^{-1}) in our study (Table 4).
621 Tohjima et al. (2002) found similar growth rates that the CH_4 at Cape Ochi-ishi and
622 Hateruma Island in1995-2000 was increased about 4.5 and 4.7 ppb yr^{-1}, respectively. In
623 early 1990s, the CH_4 trend at WLG is very low, which was similar to the global growth
624 rates (Fig. 11b). The levels of OH radicals may have controlled the decrease or increase
625 of CH_4 in the atmosphere during this period (Dlugokencky et al., 1998; Rigby et al.,
626 2017; Turner et al., 2017). The growth rates were high in 1998 (Fig. 11b), which may
627 have been due to the high temperatures, large biomass burning and weak destruction
628 (Cunnold et al., 2002; Lelieveld et al., 2004; Simmonds et al., 2005).

629 The continuously larger CH_4 growth rates after 2007 at WLG (Fig. 11), e.g., 7.6 ±
630 0.2 ppb yr^{-1} in 2008-2012, 5.7 ± 0.1 ppb yr^{-1} in 2013-2016 (Table 4), were similar to the
631 recent study by Nisbet et al. (2016) and (2019), which showed the global CH_4 increased
632 by 5.7 ± 1.2 ppb yr^{-1} in 2007-2014, and the much higher of 12.7 ± 0.5 ppb yr^{-1} in 2014,
633 10.1 ± 0.7 ppb yr^{-1} in 2015, 7.0 ± 0.7 ppb yr^{-1} in 2016 and 7.7 ± 0.7 in 2017 ppb yr^{-1}.
634 The average growth rate in the northern hemisphere was 7.3 ± 1.3 ppb in 2007 and 8.1
635 ± 1.6 ppb in 2008 (Dlugokencky et al., 2009), which was also similar to the observation
636 at WLG (Table 4). After 2007, most sites in the northern hemisphere displayed large
637 CH_4 growth rates. Fang et al. (2013) showed that the annual growth rate of CH_4 was
638 9.4 ± 0.2 ppb yr^{-1} in 2009-2011 at WLG, which were a little higher than our study in
639 similar period. The adjacent stations in China also revealed high CH_4 growth rates, e.g.,
640 8.0 ± 1.2 ppb yr^{-1} at Lin'an in 2009-2011, 7.9 ± 0.9 ppb yr^{-1} at Longfengshan in 2009-
641 2011, and 10 ± 0.1 ppb yr^{-1} at Shangdianzi in 2009-2013 (Fang et al., 2013, 2016),
642 which was higher than the similar period in 2008-2012 or 2013-2016 at WLG (Table
643 4). The CH_4 measurements in other countries, e.g., Beromünster tall tower station also
644 showed high growth rate of 9.66 ppb yr^{-1} in 2012-2014 (Satar et al., 2016). The very
645 warm temperatures, large biomass burning and the climatic anomaly e.g., El Niño, La
646 Niña event, were likely enhanced the CH_4 emissions after 2007 (Dlugokencky et al.,

https://doi.org/10.5194/acp-2020-481
Preprint. Discussion started: 29 July 2020


Atmospheric Chemistry and Physics Discussions

647 2009). Additionally, the anomalously sharply increasing or decreasing years (e.g.,
648 2007/2008) may have a significant influence on the overall CH_4 trend (Fig. 11), and
649 these frequent anomalies appeared in most long-term observation stations, e.g., MLO
650 in USA (Dlugokencky et al., 2009), Mount Zugspitze in Germany (Yuan et al., 2019),
651 which were also possibly attributed to climatic forces, such as the exception during the
652 El Niño oscillation, forest fires, volcanic eruptions, and extreme weather events
653 (Keeling et al., 1995; Dlugokencky et al., 2009; Keenan et al., 2016; Nisbet et al., 2019).
654 The study by Satar et al. (2016) at Beromünster, Switzerland explained that the short-
655 term spikes were possibly related to emissions from agricultural activities, while the
656 longer lasting peaks were because of air mass transport and mixing.

657 It is well established that the human activities are mainly responsible for the recent
658 rapid CH_4 growth rates and anomalies. The analysis from Emissions Database for
659 Global Atmospheric Research (EDGAR) showed the CH_4 emission by per sector in
660 China (Fig. S8) (Crippa et al., 2019). During the observing period, the waste, the oil
661 and natural gas and open burning continuously emitted large amount of CH_4 into the
662 air. After 2000, the CH_4 emission from solid fuel increased greatly in China. After 2003,
663 the CH_4 emitted from rice cultivation also increased continuously (Fig. S8). The
664 increased emissions from these sectors may greatly contribute to the CH_4 increase at
665 WLG, as well as the other regions in China. In addition, the recent studies reveled that
666 China's coal sector may have dominated the clearly positive trend in recent years, which
667 contributed the highest proportion of the anthropogenic CH_4 emissions (~33%)
668 (Janssens-Maenhout et al., 2019; Miller et al., 2019). In 2010-2015, China's coal
669 production increased obviously (from 3400 to 4000 million metric tons), but emissions
670 trends of CH_4 by rice, agriculture, ruminants, waste, and oil/gas have grown slightly
671 and even remained flat (EIA, USA). The isotopic evidence suggests that the significant
672 increase of biogenic emissions was the dominant factor of CH_4 rise, especially in the
673 tropical wetlands with strong rainfall anomalies, or the agricultural sources such as rice
674 paddies and ruminants, fossil fuel emissions have not been the main cause (Nisbet et

https://doi.org/10.5194/acp-2020-481
Preprint. Discussion started: 29 July 2020


Atmospheric Chemistry and Physics Discussions

675 al., 2016). The study by Chen et al. (2013) illustrated that the warming (0.2 °C per
676 decade) in the Tibetan Plateau resulted in substantial emission of CH_4 due to the
677 permafrost thawing and glaciers melting. However, up to now, the specific causes of
678 such distinct variability around the years, e.g., the spikes or near-zero CH_4 growth rates,
679 are not yet determined.
680
681 **4. 3. 3 Annual growth rate in Qinghai-Tibetan Plateau**

682 Although similar annual growth rates were found among the City Regions (CR), the
683 Tibet Plateau (TP) and total regional records (Total) in the entire observing period
684 (1994-2016) (Fig. 11), significant differences were found in short-term periods (Fig.
685 S3). In 2013-2016 (Table 4), the TP showed larger growth rate than that in CR, implying
686 stronger CH_4 source in the Tibetan Plateau in recent years. The seasonal amplitude in
687 the Tibetan Plateau was continuously increasing, which also revealed that the Tibetan
688 Plateau was intensively affected by strong regional sources. Without air mass transport
689 from the city regions, the significantly increased annual growth rate (TR) in 2008-2012
690 (10.1 ± 0.1 ppb yr^{-1}) and 2013-2016 (6.3 ± 0.1 ppb yr^{-1}) (Fig. S5 and Table 5) suggested
691 that there were possibly other strong CH_4 sources around WLG not from cities.
692 Northern India and eastern China were obviously the largest two source regions of CH_4
693 at WLG (Fig. S9) (Crippa et al., 2019). Since the Tibetan Plateau was coincidently
694 trapped in the middle of the largest increased source areas, the atmospheric CH_4 at
695 WLG was very likely dominated by long-distance transport from these two regions.
696 Although CH_4 emissions increased slowly during 1994-2002, and even negative trend
697 appeared in southeast China (Fig. S9), significantly increased emissions appeared in
698 both southeast and southwest Asia after 2007. The rapidly increased CH_4 would
699 probably make it difficult to meet the goals of carbon emission reduction in the future.
700 Especially on the scenario of quick increasing CH_4 on the Qinghai-Tibetan Plateau due
701 to the emission from two largest source regions. In view of the integrated eco-
702 environmental change processes and unique topography in the Qinghai-Tibetan

https://doi.org/10.5194/acp-2020-481
Preprint. Discussion started: 29 July 2020


Atmospheric Chemistry and Physics Discussions

703 Plateau, it may provide us one of the last precious regions to study global climate
704 changes (Chen et al., 2013). The anomalously year to year fluctuations of atmospheric
705 CH_4 in Tibetan Plateau were unquestionably a warning or alarm to the world, and the
706 unprecedented annual growth rate might be a dangerous signal to global climate change.
707

708 **5 Conclusion**

709 The atmospheric CH_4 at Mt.Waliguan increased continuously during 1994-2017.
710 Although near-zero and even negative growth appeared in some particular periods, e.g.,
711 1999-2000, and 2004-2006, the overall trend of CH_4 was increased rapidly, especially
712 in recent decade. Obvious diurnal cycle was found with the peak at noon and a trough
713 at late afternoon. Due to the unique geophysical locations and transport pathway, the
714 seasonal averages of CH_4 at WLG displayed an opposite trend with sites in the northern
715 hemisphere, with summer maximum and spring minimum. Large amount of air masses
716 was from west and northwest regions of WLG, which accompanied with higher CH_4
717 mole fractions than that from city regions. The Northern India possibly became a strong
718 source of CH_4 to WLG rather than city regions before.
719 As time goes by, the temporal patterns (e.g., seasonal amplitude), the annual
720 variations, the long-term trends or potential source distribution of CH_4 at WLG are all
721 changing. Thus, the long-term verification is extremely important to accurately
722 understand CH_4 variations. The case study in Qinghai-Tibetan Plateau revealed
723 unprecedented annual growth rates of CH_4. In recent years, the Tibetan Plateau even
724 showed larger growth rate than that in city regions. Tibetan Plateau was with the highest
725 average altitude and was almost impervious to strong human activities. There is no
726 doubt that the anomalously variation and the unprecedented annual growth rate of
727 atmospheric CH_4 in this region might be a dangerous signal to global climate change.
728
729
730

https://doi.org/10.5194/acp-2020-481
Preprint. Discussion started: 29 July 2020

Atmospheric Chemistry and Physics Discussions

Data availability. The gridded meteorological data (2004-2017) from NOAA-ARL was available at ftp://arlftp.arlhq.noaa.gov/pub/archives/gdas1/. The data from MLO, JFJ, MNM station was downloaded from World Data Centre for Greenhouse Gases (WDCGG) at https://gaw.kishou.go.jp/. The MBL data was available at ftp://aftp.cmdl.noaa.gov/data/trace_gases/CH_4/flask/surface/. The geographical distribution of annual emission data by Emissions Database for Global Atmospheric Research (EDGAR) was from website https://edgar.jrc.ec.europa.eu/overview.php?v=50_GHG.

Author contributions. SL, SF and ZF designed the research. SL performed the data processing with assistance of SF and MG. The station were monitored, maintained ML and PL, and they collected, preprocessed, and provided the hourly observational dataset. SL and SF finished the manuscript with contributions from all the co-authors.

Competing interests. The authors declare that they have no conflict of interest.

Acknowledgments. This study was funded by the National Key Research and Development Program of China (2017YFC0209700). We also thanks to the staff who have contributed to the system installation and maintenance at the Waliguan in past decades.

https://doi.org/10.5194/acp-2020-481
Preprint. Discussion started: 29 July 2020


Atmospheric Chemistry and Physics Discussions

754 **References**

755 Ashbaugh, L. L., Malm, W. C., and Sadeh, W. Z.: A residence time probability analysis
756 of sulfur concentrations at grand-canyon-national-park, Atmos. Environ., 19, 1263-
757 1270, 10.1016/0004-6981(85)90256-2, 1985.
758 Battle, M., Bender, M., Sowers, T., Tans, P. P., Butler, J. H., Elkins, J. W., Ellis, J. T.,
759 Conway, T., Zhang, N., Lang, P., and Clarke, A. D.: Atmospheric gas concentrations
760 over the past century measured in air from firn at the south pole, Nature, 383, 231-
761 235, 10.1038/383231a0, 1996.
762 Bergamaschi, P., Houweling, S., Segers, A., Krol, M., Frankenberg, C., Scheepmaker,
763 R. A., Dlugokencky, E., Wofsy, S. C., Kort, E. A., Sweeney, C., Schuck, T.,
764 Brenninkmeijer, C., Chen, H., Beck, V., and Gerbig, C.: Atmospheric CH_4 in the first
765 decade of the 21st century: Inverse modeling analysis using sciamachy satellite
766 retrievals and NOAA surface measurements, J. Geophys. Res.-Atmos., 118, 7350-
767 7369, 10.1002/jgrd.50480, 2013.
768 Blake, D. R., Mayer, E. W., Tyler, S. C., Makide, Y., Montague, D. C., and Rowland, F.
769 S.: Global increase in atmospheric methane concentrations between 1978 and 1980,
770 Geophys. Res. Lett., 9, 477-480, 10.1029/GL009i004p00477, 1982.
771 Bousquet, P., Ringeval, B., Pison, I., Dlugokencky, E. J., Brunke, E. G., Carouge, C.,
772 Chevallier, F., Fortems-Cheiney, A., Frankenberg, C., Hauglustaine, D. A.,
773 Krummel, P. B., Langenfelds, R. L., Ramonet, M., Schmidt, M., Steele, L. P., Szopa,
774 S., Yver, C., Viovy, N., and Ciais, P.: Source attribution of the changes in atmospheric
775 methane for 2006-2008, Atmos. Chem. Phys., 11, 3689-3700, 10.5194/acp-11-3689-
776 2011, 2011.
777 Cai, Z. C., Tsuruta, H., and Minami, K.: Methane emission from rice fields in China:
778 Measurements and influencing factors, J. Geophys. Res.-Atmos., 105, 17231-17242,
779 10.1029/2000jd900014, 2000.
780 Carslaw, D. C., Beevers, S. D., Ropkins, K., and Bell, M. C.: Detecting and quantifying
781 aircraft and other on-airport contributions to ambient nitrogen oxides in the vicinity

https://doi.org/10.5194/acp-2020-481
Preprint. Discussion started: 29 July 2020

782 of a large international airport, Atmos. Environ., 40, 5424-5434,
783 10.1016/j.atmosenv.2006.04.062, 2006.
784 Chen, H., Zhu, Q. A., Peng, C. H., Wu, N., Wang, Y. F., Fang, X. Q., Gao, Y. H., Zhu,
785 D., Yang, G., Tian, J. Q., Kang, X. M., Piao, S. L., Ouyang, H., Xiang, W. H., Luo,
786 Z. B., Jiang, H., Song, X. Z., Zhang, Y., Yu, G. R., Zhao, X. Q., Gong, P., Yao, T. D.,
787 and Wu, J. H.: The impacts of climate change and human activities on
788 biogeochemical cycles on the Qinghai-Tibetan Plateau, Glob. Change Biol., 19,
789 2940-2955, 10.1111/gcb.12277, 2013.
790 Crippa, M., Oreggioni, G., Guizzardi, D., Muntean, M., Schaaf, E., Lo Vullo, E.,
791 Solazzo, E., Monforti-Ferrario, F., Olivier, J.G.J., Vignati, E.: Fossil CO_2 and GHG
792 emissions of all world countries - 2019 Report, EUR 29849 EN, Publications Office
793 of the European Union, Luxembourg, ISBN 978-92-76-11100-9.
794 https://edgar.jrc.ec.europa.eu/overview.php?v=50_GHG, 2019.
795 Cunnold, D. M., Steele, L. P., Fraser, P. J., Simmonds, P. G., Prinn, R. G., Weiss, R. F.,
796 Porter, L. W., O'Doherty, S., Langenfelds, R. L., Krummel, P. B., Wang, H. J.,
797 Emmons, L., Tie, X. X., and Dlugokencky, E. J.: In situ measurements of
798 atmospheric methane at GAGE/AGAGE sites during 1985-2000 and resulting source
799 inferences, J. Geophys. Res.-Atmos., 107, 20, 10.1029/2001jd001226, 2002.
800 Diederich, A.: Generalized additive models. An introduction with R, J. Math. Psychol.,
801 51, 339-339, 2007.
802 Dlugokencky, E. J., Steele, L. P., Lang, P. M., and Masarie, K. A.: The growth-rate and
803 distribution of atmospheric methane, J. Geophys. Res.-Atmos., 99, 17021-17043,
804 10.1029/94jd01245, 1994.
805 Dlugokencky, E. J., Steele, L. P., Lang, P. M., and Masarie, K. A.: Atmospheric methane
806 at Mauna-Loa and Barrow observatories - presentation and analysis of in-situ
807 measurements, J. Geophys. Res.-Atmos., 100, 23103-23113, 10.1029/95jd02460,
808 1995.
809 Dlugokencky, E. J., Masarie, K. A., Lang, P. M., and Tans, P. P.: Continuing decline in

https://doi.org/10.5194/acp-2020-481
Preprint. Discussion started: 29 July 2020


Atmospheric Chemistry and Physics Discussions

the growth rate of the atmospheric methane burden, Nature, 393, 447-450, 10.1038/30934, 1998.

Dlugokencky, E. J., Bruhwiler, L., White, J. W. C., Emmons, L. K., Novelli, P. C., Montzka, S. A., Masarie, K. A., Lang, P. M., Crotwell, A. M., Miller, J. B., and Gatti, L. V.: Observational constraints on recent increases in the atmospheric CH_4 burden, Geophys. Res. Lett., 36, 5, 10.1029/2009gl039780, 2009.

Dlugokencky, E.J., Crotwell, A.M., Lang, P.M., and Mund, J.W.: Atmospheric Methane Dry Air Mole Fractions from quasi-continuous measurements at Barrow, Alaska and Mauna Loa, Hawaii, 1986-2018, Version: 2019-03-04, Path: ftp://aftp.cmdl.noaa.gov/data/trace_gases/CH_4/in-situ/surface/, 2019a.

Dlugokencky, E.J., Lang, P.M., Crotwell, A.M., Thoning, K.W., and M.J. Crotwell.: Atmospheric Methane Dry Air Mole Fractions from the NOAA ESRL Carbon Cycle Cooperative Global Air Sampling Network. Data Path: ftp://aftp.cmdl.noaa.gov/data/trace_gases/CH_4/flask/surface/, 2019b.

Draxier, R. R., and Hess, G. D.: An overview of the hysplit_4 modelling system for trajectories, dispersion and deposition, Aust. Meteorol. Mag., 47, 295-308, 1998.

Etheridge, D. M., Steele, L. P., Francey, R. J., and Langenfelds, R. L.: Atmospheric methane between 1000 AD and present: Evidence of anthropogenic emissions and climatic variability, J. Geophys. Res.-Atmos., 103, 15979-15993, 10.1029/98jd00923, 1998.

Etminan, M., Myhre, G., Highwood, E. J., and Shine, K. P.: Radiative forcing of carbon dioxide, methane, and nitrous oxide: A significant revision of the methane radiative forcing, Geophys. Res. Lett., 43, 12614-12623, 10.1002/2016gl071930, 2016.

Fang, S. X., Zhou, L. X., Masarie, K. A., Xu, L., and Rella, C. W.: Study of atmospheric CH_4 mole fractions at three WMO/GAW stations in China, J. Geophys. Res.-Atmos., 118, 4874-4886, 10.1002/jgrd.50284, 2013.

Fang, S. X., Tans, P. P., Dong, F., Zhou, H. G., and Luan, T.: Characteristics of atmospheric CO_2 and CH_4 at the Shangdianzi regional background station in China,

https://doi.org/10.5194/acp-2020-481
Preprint. Discussion started: 29 July 2020


Atmospheric Chemistry and Physics Discussions

838 Atmos. Environ., 131, 1-8, 10.1016/j.atmosenv.2016.01.044, 2016.
839 Fu, X. W., Feng, X., Liang, P., Zhang, H., Ji, J., and Liu, P.: Temporal trend and sources
840 of speciated atmospheric mercury at Waliguan GAW station, northwestern China,
841 Atmos. Chem. Phys., 12, 1951-1964, 10.5194/acp-12-1951-2012, 2012.
842 Galloway, J. N.: Atmospheric acidification - projections for the future, Ambio, 18, 161-
843 166, 1989.
844 Hausmann, P., Sussmann, R., and Smale, D.: Contribution of oil and natural gas
845 production to renewed increase in atmospheric methane (2007-2014): Top-down
846 estimate from ethane and methane column observations, Atmos. Chem. Phys., 16,
847 3227-3244, 10.5194/acp-16-3227-2016, 2016.
848 IPCC, Climate Change 2014: Synthesis Report. Contribution of Working Groups I, II
849 and III to the Fifth Assessment Report of the Intergovernmental Panel on Climate
850 Change [Core Writing Team, R.K. Pachauri and L.A. Meyer (eds.)]. IPCC, Geneva,
851 Switzerland, 151 pp, 2014.
852 Janssens-Maenhout, G., Crippa, M., Guizzardi, D., Muntean, M., Schaaf, E., Dentener,
853 F., Bergamaschi, P., Pagliari, V., Olivier, J. G. J., Peters, J., van Aardenne, J. A.,
854 Monni, S., Doering, U., Petrescu, A. M. R., Solazzo, E., and Oreggioni, G. D.: Edgar
855 v4.3.2 global atlas of the three major greenhouse gas emissions for the period 1970-
856 2012, Earth Syst. Sci. Data, 11, 959-1002, 10.5194/essd-11-959-2019, 2019.
857 Keeling, C. D., Bacastow, R. B., Bainbridge, A. E., Ekdahl, C. A., Guenther, P. R.,
858 Waterman, L. S., and Chin, J. F. S.: Atmospheric carbon-dioxide variations at Mauna-
859 Loa observatory, Hawaii, Tellus, 28, 538-551, 1976.
860 Keeling, C. D., Whorf, T. P., Wahlen, M., and Vanderplicht, J.: Interannual extremes in
861 the rate of rise of atmospheric carbon-dioxide since 1980, Nature, 375, 666-670,
862 10.1038/375666a0, 1995.
863 Keenan, T. F., Prentice, I. C., Canadell, J. G., Williams, C. A., Wang, H., Raupach, M.,
864 and Collatz, G. J.: Recent pause in the growth rate of atmospheric CO_2 due to
865 enhanced terrestrial carbon uptake, Nat. Commun., 7, 9, 10.1038/ncomms13428,

https://doi.org/10.5194/acp-2020-481
Preprint. Discussion started: 29 July 2020


Atmospheric Chemistry and Physics Discussions

2016.

Lelieveld, J., Dentener, F. J., Peters, W., and Krol, M. C.: On the role of hydroxyl radicals in the self-cleansing capacity of the troposphere, Atmos. Chem. Phys., 4, 2337-2344, 10.5194/acp-4-2337-2004, 2004.

Lin, M. Y., Horowitz, L. W., Oltmans, S. J., Fiore, A. M., and Fan, S. M.: Tropospheric ozone trends at Mauna Loa observatory tied to decadal climate variability, Nat. Geosci., 7, 136-143, 10.1038/ngeo2066, 2014.

Liu, S., Fang, S. X., Liang, M., Ma, Q. L., and Feng, Z. Z.: Study on CO data filtering approaches based on observations at two background stations in China, Sci. Total Environ., 691, 675-684, 10.1016/j.scitotenv.2019.07.162, 2019.

Logan, J. A., Prather, M. J., Wofsy, S. C., and McElroy, M. B.: Tropospheric chemistry - a global perspective, J. Geophys. Res.-Oceans, 86, 7210-7254, 10.1029/JC086iC08p07210, 1981.

Loov, J. M. B., Henne, S., Legreid, G., Staehelin, J., Reimann, S., Prevot, A. S. H., Steinbacher, M., and Vollmer, M. K.: Estimation of background concentrations of trace gases at the Swiss Alpine site Jungfraujoch (3580 m asl), J. Geophys. Res.-Atmos., 113, 17, 10.1029/2007jd009751, 2008.

Ma, J. Z., Tang, J., Zhou, X. J., and Zhang, X. S.: Estimates of the chemical budget for ozone at Waliguan observatory, J. Atmos. Chem., 41, 21-48, 10.1023/a:1013892308983, 2002.

Matsueda, H. et al., Methane standard gases for atmospheric measurements at the MRI and JMA and intercomparison experiments, Pap. Meteor. Geophys., 54, 91-109, 2004.

Miller, S. M., Michalak, A. M., Detmers, R. G., Hasekamp, O. P., Bruhwiler, L. M. P., and Schwietzke, S.: China's coal mine methane regulations have not curbed growing emissions, Nat. Commun., 10, 8, 10.1038/s41467-018-07891-7, 2019.

Nisbet, E. G., Dlugokencky, E. J., and Bousquet, P.: Methane on the rise-again, Science, 343, 493-495, 10.1126/science.1247828, 2014.

https://doi.org/10.5194/acp-2020-481
Preprint. Discussion started: 29 July 2020


Atmospheric Chemistry and Physics Discussions

894 Nisbet, E. G., Dlugokencky, E. J., Manning, M. R., Lowry, D., Fisher, R. E., France, J.
895 L., Michel, S. E., Miller, J. B., White, J. W. C., Vaughn, B., Bousquet, P., Pyle, J. A.,
896 Warwick, N. J., Cain, M., Brownlow, R., Zazzeri, G., Lanoisellé, M., Manning, A.
897 C., Gloor, E., Worthy, D. E. J., Brunke, E.-G., Labuschagne, C., Wolff, E. W., and
898 Ganesan, A. L.: Rising atmospheric methane: 2007-2014 growth and isotopic shift,
899 Global Biogeochem. Cy., 30, 1356-1370, 10.1002/2016gb005406, 2016.
900 Nisbet, E. G., Manning, M. R., Dlugokencky, E. J., Fisher, R. E., Lowry, D., Michel, S.
901 E., Myhre, C. L., Platt, S. M., Allen, G., Bousquet, P., Brownlow, R., Cain, M.,
902 France, J. L., Hermansen, O., Hossaini, R., Jones, A. E., Levin, I., Manning, A. C.,
903 Myhre, G., Pyle, J. A., Vaughn, B. H., Warwick, N. J., and White, J. W. C.: Very
904 strong atmospheric methane growth in the 4 years 2014-2017: Implications for the
905 paris agreement, Global Biogeochem. Cy., 33, 318-342, 10.1029/2018gb006009,
906 2019.
907 Pearman, G. I., and Beardsmore, D. J.: Atmospheric carbon-dioxide measurements in
908 the Australian region - 10 years of aircraft data, Tellus Ser. B-Chem. Phys. Meteorol.,
909 36, 1-24, 10.1111/j.1600-0889.1984.tb00047.x, 1984.
910 Polissar, A. V., Hopke, P. K., Paatero, P., Kaufmann, Y. J., Hall, D. K., Bodhaine, B. A.,
911 Dutton, E. G., and Harris, J. M.: The aerosol at barrow, alaska: Long-term trends and
912 source locations, Atmos. Environ., 33, 2441-2458, 10.1016/s1352-2310(98)00423-
913 3, 1999.
914 Popa, M. E., Gloor, M., Manning, A. C., Jordan, A., Schultz, U., Haensel, F., Seifert,
915 T., and Heimann, M.: Measurements of greenhouse gases and related tracers at
916 Bialystok tall tower station in Poland, Atmos. Meas. Tech., 3, 407-427, 10.5194/amt-
917 3-407-2010, 2010.
918 Press, W. H., Flannery, B. P., Teukolsky, S. A., and Vetterling, W. T.: Numerical recipes
919 in C: The art of scientific programming, Section, 10, 408-412, 1992.
920 Rasmussen, R. A., and Khalil, M. A. K.: Atmospheric methane in the recent and ancient
921 atmospheres - concentrations, trends, and interhemispheric gradient, J. Geophys.

https://doi.org/10.5194/acp-2020-481
Preprint. Discussion started: 29 July 2020


Atmospheric Chemistry and Physics Discussions

922 Res.-Atmos., 89, 1599-1605, 10.1029/JD089iD07p11599, 1984.
923 R Core Team.: R: a language and environment for statistical computing. R Foundation
924 for Statistical Computing, Vienna, Austria, URL: http://www.R-project.org/, 2020.
925 Rigby, M., Montzka, S. A., Prinn, R. G., White, J. W. C., Young, D., O'Doherty, S.,
926 Lunt, M. F., Ganesan, A. L., Manning, A. J., Simmonds, P. G., Salameh, P. K., Harth,
927 C. M., Muhle, J., Weiss, R. F., Fraser, P. J., Steele, L. P., Krummel, P. B., McCulloch,
928 A., and Park, S.: Role of atmospheric oxidation in recent methane growth, Proc. Natl.
929 Acad. Sci. U. S. A., 114, 5373-5377, 10.1073/pnas.1616426114, 2017.
930 Rousseau, D. D., Duzer, D., Etienne, J. L., Cambon, G., Jolly, D., Ferrier, J., and
931 Schevin, P.: Pollen record of rapidly changing air trajectories to the North Pole, J.
932 Geophys. Res.-Atmos., 109, 10.1029/2003jd003985, 2004.
933 Rubino, M., Etheridge, D. M., Thornton, D. P., Howden, R., Allison, C. E., Francey, R.
934 J., Langenfelds, R. L., Steele, L. P., Trudinger, C. M., Spencer, D. A., Curran, M. A.
935 J., van Ommen, T. D., and Smith, A. M.: Revised records of atmospheric trace gases
936 CO_2, CH_4, N_2O, and delta C-13-CO_2 over the last 2000 years from Law Dome,
937 Antarctica, Earth Syst. Sci. Data, 11, 473-492, 10.5194/essd-11-473-2019, 2019.
938 Satar, E., Berhanu, T. A., Brunner, D., Henne, S., and Leuenberger, M.: Continuous
939 CO_2/CH_4/CO measurements (2012-2014) at Beromunster tall tower station in
940 Switzerland, Biogeosciences, 13, 2623-2635, 10.5194/bg-13-2623-2016, 2016.
941 Saunois, M., Bousquet, P., Poulter, B., Peregon, A., Ciais, P., Canadell, J. G.,
942 Dlugokencky, E. J., Etiope, G., Bastviken, D., Houweling, S., Janssens-Maenhout,
943 G., Tubiello, F. N., Castaldi, S., Jackson, R. B., Alexe, M., Arora, V. K., Beerling, D.
944 J., Bergamaschi, P., Blake, D. R., Brailsford, G., Brovkin, V., Bruhwiler, L.,
945 Crevoisier, C., Crill, P., Covey, K., Curry, C., Frankenberg, C., Gedney, N., Hoglund-
946 Isaksson, L., Ishizawa, M., Ito, A., Joos, F., Kim, H. S., Kleinen, T., Krummel, P.,
947 Lamarque, J. F., Langenfelds, R., Locatelli, R., Machida, T., Maksyutov, S.,
948 McDonald, K. C., Marshall, J., Melton, J. R., Morino, I., Naik, V., O'Doherty, S.,
949 Parmentier, F. J. W., Patra, P. K., Peng, C. H., Peng, S. S., Peters, G. P., Pison, I.,

https://doi.org/10.5194/acp-2020-481
Preprint. Discussion started: 29 July 2020


Atmospheric Chemistry and Physics Discussions

950 Prigent, C., Prinn, R., Ramonet, M., Riley, W. J., Saito, M., Santini, M., Schroeder,
951 R., Simpson, I. J., Spahni, R., Steele, P., Takizawa, A., Thornton, B. F., Tian, H. Q.,
952 Tohjima, Y., Viovy, N., Voulgarakis, A., van Weele, M., van der Werf, G. R., Weiss,
953 R., Wiedinmyer, C., Wilton, D. J., Wiltshire, A., Worthy, D., Wunch, D., Xu, X. Y.,
954 Yoshida, Y., Zhang, B., Zhang, Z., and Zhu, Q.: The global methane budget 2000-
955 2012, Earth Syst. Sci. Data, 8, 697-751, 10.5194/essd-8-697-2016, 2016.
956 Saunois, M., Stavert, A.R., Poulter, B. et al.: The Global Methane Budget 2000-2017,
957 Earth Syst. Sci. Data, https://doi.org/10.5194/essd-2019-128, 2019.
958 Schaefer, H., Fletcher, S. E. M., Veidt, C., Lassey, K. R., Brailsford, G. W., Bromley, T.
959 M., Dlugokencky, E. J., Michel, S. E., Miller, J. B., Levin, I., Lowe, D. C., Martin,
960 R. J., Vaughn, B. H., and White, J. W. C.: A 21st-century shift from fossil-fuel to
961 biogenic methane emissions indicated by (CH_4)-C-13, Science, 352, 80-84,
962 10.1126/science.aad2705, 2016.
963 Simmonds, P. G., Manning, A. J., Derwent, R. G., Ciais, P., Ramonet, M., Kazan, V.,
964 and Ryall, D.: A burning question. Can recent growth rate anomalies in the
965 greenhouse gases be attributed to large-scale biomass burning events?, Atmos.
966 Environ., 39, 2513-2517, 10.1016/j.atmosenv.2005.02.018, 2005.
967 Streets, D. G., and Waldhoff, S. T.: Present and future emissions of air pollutants in
968 china: SO_2, NO_x, and CO, Atmos. Environ., 34, 363-374, 10.1016/s1352-
969 2310(99)00167-3, 2000.
970 Thompson, R. L., Manning, A. C., Gloor, E., Schultz, U., Seifert, T., Hansel, F., Jordan,
971 A., and Heimann, M.: In-situ measurements of oxygen, carbon monoxide and
972 greenhouse gases from Ochsenkopf tall tower in Germany, Atmos. Meas. Tech., 2,
973 573-591, 10.5194/amt-2-573-2009, 2009.
974 Tohjima, Y., Machida, T., Utiyama, M., Katsumoto, M., Fujinuma, Y., and Maksyutov,
975 S.: Analysis and presentation of in situ atmospheric methane measurements from
976 Cape Ochi-ishi and Hateruma island, J. Geophys. Res.-Atmos., 107, 11,
977 10.1029/2001jd001003, 2002.

https://doi.org/10.5194/acp-2020-481
Preprint. Discussion started: 29 July 2020

978 Tohjima, Y., Kubo, M., Minejima, C., Mukai, H., Tanimoto, H., Ganshin, A.,
979 Maksyutov, S., Katsumata, K., Machida, T., and Kita, K.: Temporal changes in the
980 emissions of CH_4 and CO from China estimated from CH_4/CO_2 and CO/CO_2
981 correlations observed at Hateruma island, Atmos. Chem. Phys., 14, 1663-1677,
982 10.5194/acp-14-1663-2014, 2014.
983 Thoning, K. W., Tans, P. P., and Komhyr, W. D.: Atmospheric carbon dioxide at Mauna
984 Loa observatory: 2. Analysis of the NOAA GMCC data, 1974-1985, J. Geophys.
985 Res.-Atmos., 94, 8549-8565, 10.1029/JD094iD06p08549, 1989.
986 Tsutsumi, Y., Mori, K., Ikegami, M., Tashiro, T., and Tsuboi, K.: Long-term trends of
987 greenhouse gases in regional and background events observed during 1998-2004 at
988 Yonagunijima located to the east of the Asian continent, Atmos. Environ., 40, 5868-
989 5879, 10.1016/j.atmosenv.2006.04.036, 2006.
990 Turner, A. J., Frankenbergb, C., Wennberg, P. O., and Jacob, D. J.: Ambiguity in the
991 causes for decadal trends in atmospheric methane and hydroxyl, Proc. Natl. Acad.
992 Sci. U. S. A., 114, 5367-5372, 10.1073/pnas.1616020114, 2017.
993 Uria-Tellaetxe, I., and Carslaw, D. C.: Conditional bivariate probability function for
994 source identification, Environ. Modell. Softw., 59, 1-9,
995 10.1016/j.envsoft.2014.05.002, 2014.
996 US EIA (US Energy Information Administration): International energy statistics,
997 available at https://www.eia.gov/ beta/international/data/browser/.
998 Vaghjiani, G. L., and Ravishankara, A. R.: New measurement of the rate coefficient for
999 the reaction of OH with methane, Nature, 350, 406-409, 10.1038/350406a0, 1991.
1000 Wada, A., Sawa, Y., Matsueda, H., Taguchi, S., Murayama, S., Okubo, S., and Tsutsumi,
1001 Y.: Influence of continental air mass transport on atmospheric CO_2 in the western
1002 North Pacific, J. Geophys. Res.-Atmos., 112, 12, 10.1029/2006jd007552, 2007.
1003 Wang, D. Q., Chen, Z. L., and Xu, S. Y.: Methane emission from Yangtze estuarine
1004 wetland, china, J. Geophys. Res.-Biogeosci., 114, 11, 10.1029/2008jg000857, 2009.
1005 Wang, T., Cheung, T. F., Li, Y. S., Yu, X. M., and Blake, D. R.: Emission characteristics

https://doi.org/10.5194/acp-2020-481
Preprint. Discussion started: 29 July 2020

of CO, NO_X, SO_2 and indications of biomass burning observed at a rural site in eastern China, J. Geophys. Res.-Atmos., 107, 10, 10.1029/2001jd000724, 2002.

Weber, T., Wiseman, N. A., and Kock, A.: Global ocean methane emissions dominated by shallow coastal waters, Nat. Commun., 10, 10, 10.1038/s41467-019-12541-7, 2019.

Wilson, M. C., and Smith, A. T.: The pika and the watershed: The impact of small mammal poisoning on the ecohydrology of the Qinghai-Tibetan Plateau, Ambio, 44, 16-22, 10.1007/s13280-014-0568-x, 2015.

WMO, WMO Greenhouse Gas Bulletin No.15, 2019.

WMO, WMO World Data Centre for Greenhouse Gases (WDCGG) Data Summary: Greenhouse Gases and Other Atmospheric Gases, No. 43. Japan Meteorological Agency, avaliablle at https://gaw.kishou.go.jp/static/publications/summary/sum43/sum43.pdf, 2020.

Wolf, J., Asrar, G. R., and West, T. O.: Revised methane emissions factors and spatially distributed annual carbon fluxes for global livestock, Carbon Balanc. Manag., 12, 24, 10.1186/s13021-017-0084-y, 2017.

Xiong, X., Houweling, S., Wei, J., Maddy, E., Sun, F., and Barnet, C.: Methane plume over South Asia during the monsoon season: Satellite observation and model simulation, Atmos. Chem. Phys., 9, 783-794, 10.5194/acp-9-783-2009, 2009.

Yuan, Y., Ries, L., Petermeier, H., Trickl, T., Leuchner, M., Couret, C., Sohmer, R., Meinhardt, F., and Menzel, A.: On the diurnal, weekly, and seasonal cycles and annual trends in atmospheric CO_2 at Mount Zugspitze, Germany, during 1981-2016, Atmos. Chem. Phys., 19, 999-1012, 10.5194/acp-19-999-2019, 2019.

Zellweger, C., Emmenegger, L., Firdaus, M., Hatakka, J., Heimann, M., Kozlova, E., Spain, T. G., Steinbacher, M., van der Schoot, M. V., and Buchmann, B.: Assessment of recent advances in measurement techniques for atmospheric carbon dioxide and methane observations, Atmos. Meas. Tech., 9, 4737-4757, 10.5194/amt-9-4737-2016, 2016.

https://doi.org/10.5194/acp-2020-481
Preprint. Discussion started: 29 July 2020

1034 Zhang, F., Zhou, L. X., Novelli, P. C., Worthy, D. E. J., Zellweger, C., Klausen, J., Ernst,
1035 M., Steinbacher, M., Cai, Y. X., Xu, L., Fang, S. X., and Yao, B.: Evaluation of in
1036 situ measurements of atmospheric carbon monoxide at Mount Waliguan, china,
1037 Atmos. Chem. Phys., 11, 5195-5206, 10.5194/acp-11-5195-2011, 2011.
1038 Zhang, F., Zhou, L., and Xu, L.: Temporal variation of atmospheric CH_4 and the
1039 potential source regions at Waliguan, China, Sci. China Earth Sci., 56, 727-736,
1040 10.1007/s11430-012-4577-y, 2013.
1041 Zhou, L., Worthy, D. E. J., Lang, P. M., Ernst, M. K., Zhang, X. C., Wen, Y. P., and Li,
1042 J. L.: Ten years of atmospheric methane observations at a high elevation site in
1043 western China, Atmos. Environ., 38, 7041-7054, 10.1016/j.atmosenv.2004.02.072,
1044 2004.
1045 Zhou, L. X., Conway, T. J., White, J. W. C., Mukai, H., Zhang, X. C., Wen, Y. P., Li, J.
1046 L., and MacClune, K.: Long-term record of atmospheric CO_2 and stable isotopic
1047 ratios at Waliguan observatory: Background features and possible drivers, 1991-
1048 2002, Global Biogeochem. Cy., 19, 9, 10.1029/2004gb002430, 2005.
1049 Zhou, L. X., Tang, J., Wen, Y. P., Li, J. L., Yan, P., and Zhang, X. C.: The impact of
1050 local winds and long-range transport on the continuous carbon dioxide record at
1051 Mount Waliguan, China, Tellus Ser. B-Chem. Phys. Meteorol., 55, 145-158,
1052 10.1034/j.1600-0889.2003.00064.x, 2003.
1053 Zou, J. W., Huang, Y., Jiang, J. Y., Zheng, X. H., and Sass, R. L.: A 3-year field
1054 measurement of methane and nitrous oxide emissions from rice paddies in China:
1055 Effects of water regime, crop residue, and fertilizer application, Global Biogeochem.
1056 Cy., 19, 9, 10.1029/2004gb002401, 2005.

https://doi.org/10.5194/acp-2020-481
Preprint. Discussion started: 29 July 2020

Atmospheric Chemistry and Physics Discussions

Table 1. The statistics for cluster analysis result for both CH_4 and CO at WLG station. The clusters from urban areas are highlighted with face bold.

	Cluster	Number	Average CH_4 mole fraction
Spring	**1**	**1243**	**1853.4 ± 2.7**
	2	685	1852.6 ± 3.4
	3	2231	1877.6 ± 2.5
	4	**1093**	**1850.5 ± 2.2**
	5	4108	1860.8 ± 1.5
Summer	**1**	**3981**	**1869.9 ± 1.2**
	2	2244	1878.5 ± 2.6
	3	**1040**	**1866.3 ± 2.6**
	4	916	1857.8 ± 2.4
	5	578	1876.3 ± 5.1
Autumn	**1**	**1133**	**1870.1 ± 3.7**
	2	4235	1868.8 ± 1.3
	3	2745	1873.6 ± 1.6
	4	550	1865.2 ± 3.6
Winter	1	3066	1879.8 ± 2.1
	2	**601**	**1872.6 ± 3.4**
	3	5261	1865.8 ± 1.0

https://doi.org/10.5194/acp-2020-481
Preprint. Discussion started: 29 July 2020

Atmospheric Chemistry and Physics Discussions

Table 2. The statistics of filtered CH_4 data series over different periods during 1994-2017 at WLG station.

Year	Regional representative			Local representative		
	Hours	Percentage (%)	Mean (ppb)	Hours	Percentage (%)	Mean (ppb)
1994-1997	6481	46.9	1801.7 ± 0.5	7346	53.1	1806.1 ± 0.5
1998-2002	5332	47.6	1832.6 ± 0.7	5877	52.4	1837.9 ± 0.6
2003-2007	12421	49.2	1832.2 ± 0.3	12850	50.8	1839.2 ± 0.3
2008-2012	11314	49.2	1856.4 ± 0.4	11664	50.8	1867.0 ± 0.4
2013-2017	10140	43.6	1894.9 ± 0.5	13121	56.4	1907.4 ± 0.5
1994-2017	45688	47.3	1847.9 ± 0.3	50858	52.7	1858.2 ± 0.4

https://doi.org/10.5194/acp-2020-481
Preprint. Discussion started: 29 July 2020

Atmospheric Chemistry and Physics Discussions

1063 **Table 3.** Yearly average CH_4 mole fractions at WLG station.

Year	Mean (ppb)	year	Mean (ppb)
1995	1805.8 ± 0.1	2006	1835.6 ± 0.2
1996	1804.6 ± 0.2	2007	1839.9 ± 0.5
1997	1806.8 ± 0.2	2008	1865.9 ± 0.3
1998	1827.0 ± 0.1	2009	1849.1 ± 0.1
1999	1820.2 ± 0.1	2010	1857.9 ± 0.2
2000	1820.0 ± 0.2	2011	1872.6 ± 0.4
2001	1849.2 ± 0.4	2012	1881.2 ± 0.3
2002	1835.5 ± 0.2	2013	1896.3 ± 0.2
2003	1842.5 ± 0.3	2014	1890.4 ± 0.1
2004	1836.7 ± 0.1	2015	1905.6 ± 0.3
2005	1837.4 ± 0.1	2016	1903.8 ± 0.1

1064

https://doi.org/10.5194/acp-2020-481
Preprint. Discussion started: 29 July 2020

Atmospheric Chemistry and Physics Discussions

1065 **Table 4.** Annual growth rates of atmospheric CH_4 in the City Regions (CR), the Tibet Plateau (TP),

1066 and original total regional records (Total) during 1994-2016 at WLG station.

	1994-1997	1998-2002	2003-2007	2008-2012	2013-2016	1994-2016
CR	2.8 ± 0.1	3.6 ± 0.2	5.6 ± 0.2	7.1 ± 0.2	5.5 ± 0.1	5.0 ± 0.1
TP	3.4 ± 0.1	3.0 ± 0.2	6.8 ± 0.2	5.6 ± 0.2	7.3 ± 0.1	5.2 ± 0.1
Total	4.6 ± 0.1	2.6 ± 0.2	5.3 ± 0.2	7.6 ± 0.2	5.7 ± 0.1	5.1 ± 0.1

1067

https://doi.org/10.5194/acp-2020-481
Preprint. Discussion started: 29 July 2020

Atmospheric Chemistry and Physics Discussions

1068 **Table 5.** The statistics of CH_4 data without air mass transport from city regions (TR) over different

1069 periods during 2005-2016 at WLG station.

	Transport regions	Hours	Percentage (%)	Average (ppb)	Updated growth rate (ppb yr-1)
2005-2007	TR	6922	77.2	1824.9 ± 0.2	2.7 ± 0.2
	City	2041	22.8	1835.9 ± 0.5	-
2008-2012	TR	7060	64.4	1853.7 ± 0.2	10.1 ± 0.1
	City	4254	35.6	1861.0 ± 0.3	-
2013-2016	TR	4152	61.6	1888.2 ± 0.3	6.3 ± 0.1
	City	2591	38.4	1888.5 ± 0.5	-
2005-2016	TR	18134	67.1	1850.6 ± 0.2	7.0 ± 0.1
	City	8886	32.9	1863.2 ± 0.3	-

1070

https://doi.org/10.5194/acp-2020-481
Preprint. Discussion started: 29 July 2020

Atmospheric Chemistry and Physics Discussions

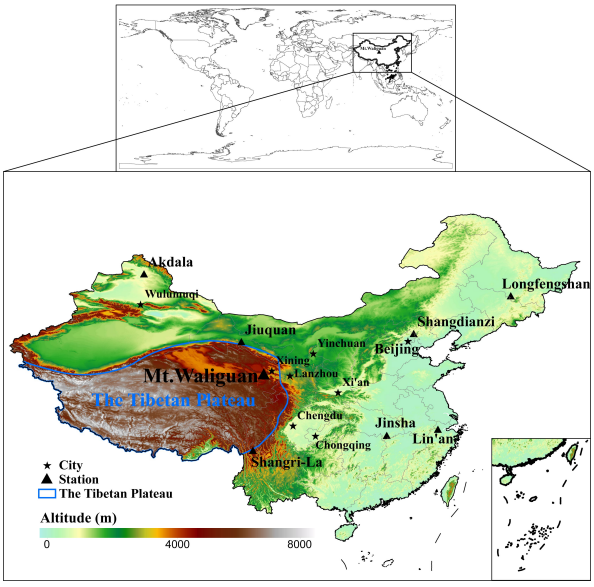

Figure 1. Location of Mt.Waliguan WMO/GAW global station as well as other regional stations in China. The gradient color indicates altitude. The digital elevation model (DEM) was downloaded from Geospatial Data Cloud site, Computer Network Information Center, Chinese Academy of Sciences (http://www.gscloud.cn), and then processed by ArcGis software. The China map was derived from © National basic Geomatics Center of China (http://www.ngcc.cn/ngcc/). The world map was obtained from © OpenStreetMap (https://www.openstreetmap.org/). And the other shpfile file data and entire map were created by ArcGis software.

https://doi.org/10.5194/acp-2020-481
Preprint. Discussion started: 29 July 2020

Atmospheric Chemistry and Physics Discussions

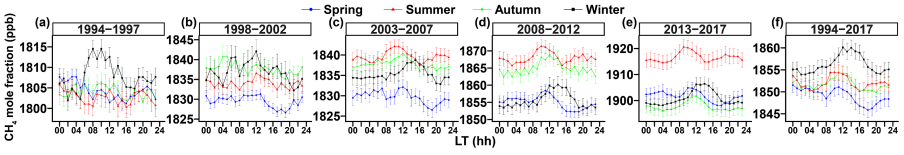

Figure 2. Diurnal CH_4 cycles in different periods from 1994 to 2017 at WLG station. The lines with different colors represent various seasons. Error bars indicate the 95% confidence intervals.

https://doi.org/10.5194/acp-2020-481
Preprint. Discussion started: 29 July 2020

Atmospheric Chemistry and Physics Discussions

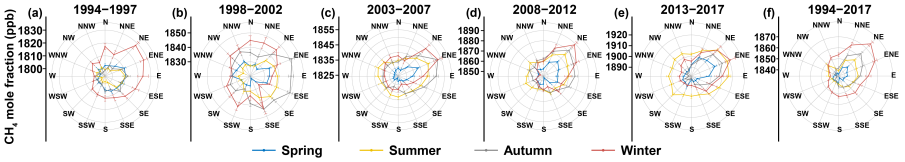

Figure 3. Wind-rose distribution of average hourly CH_4 records from 16 horizontal wind directions over different periods in 1994-2017 at WLG station. The different colors represent the CH_4 data in different seasons. Error bars in all directions indicate 95% confidence intervals.

https://doi.org/10.5194/acp-2020-481
Preprint. Discussion started: 29 July 2020

Atmospheric Chemistry and Physics Discussions

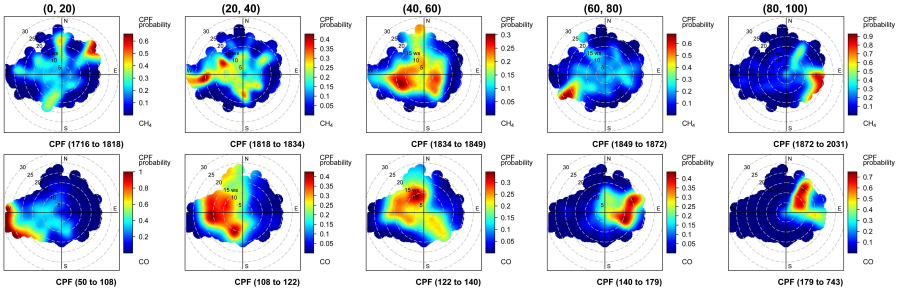

Figure 4. The polar plot of the distribution of CH_4 and CO concentration probability in different percentile ranges at WLG station. The analysis was based on the conditional probability functions (CPF) by Ashbaugh et al. (1985). The top plots show the measurements of CH_4 from 1994 to 2017. The bottom plots show the CO measurements in 2004-2017. 'ws' means the wind speed. The values in the bottom of each panel show the range of concentration in relevant percentile range. Gradient colors represent the levels of CPF probability in different percentile ranges.

https://doi.org/10.5194/acp-2020-481
Preprint. Discussion started: 29 July 2020

Atmospheric Chemistry and Physics Discussions

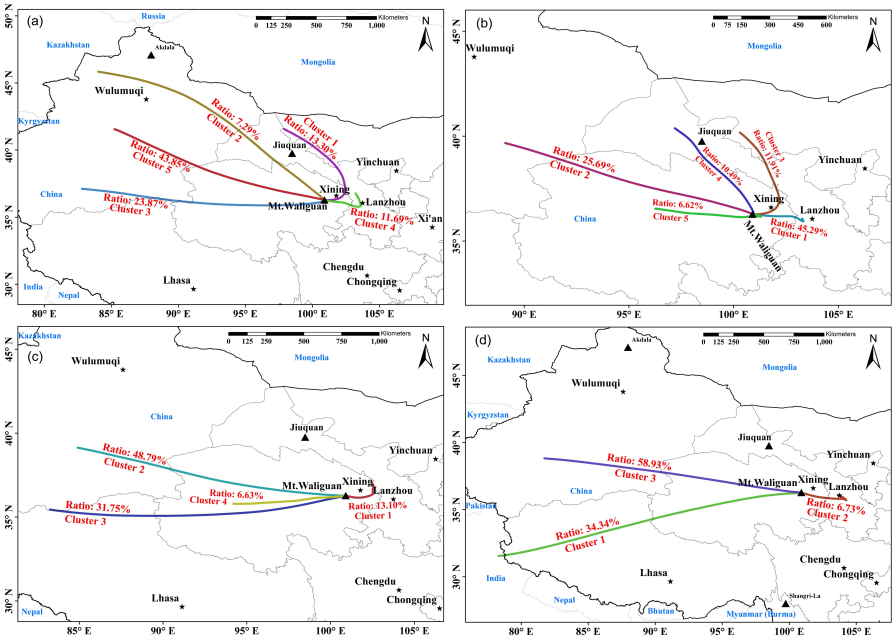

Figure 5. Cluster analysis to the 72-h back trajectories in different seasons during 2004-2017 ending at WLG station. The (a), (b), (c) and (d) represents spring, summer, autumn and winter, respectively. The lines with different colors denote different cluster analysis results. The proportion of trajectories on each cluster is also marked.

https://doi.org/10.5194/acp-2020-481
Preprint. Discussion started: 29 July 2020

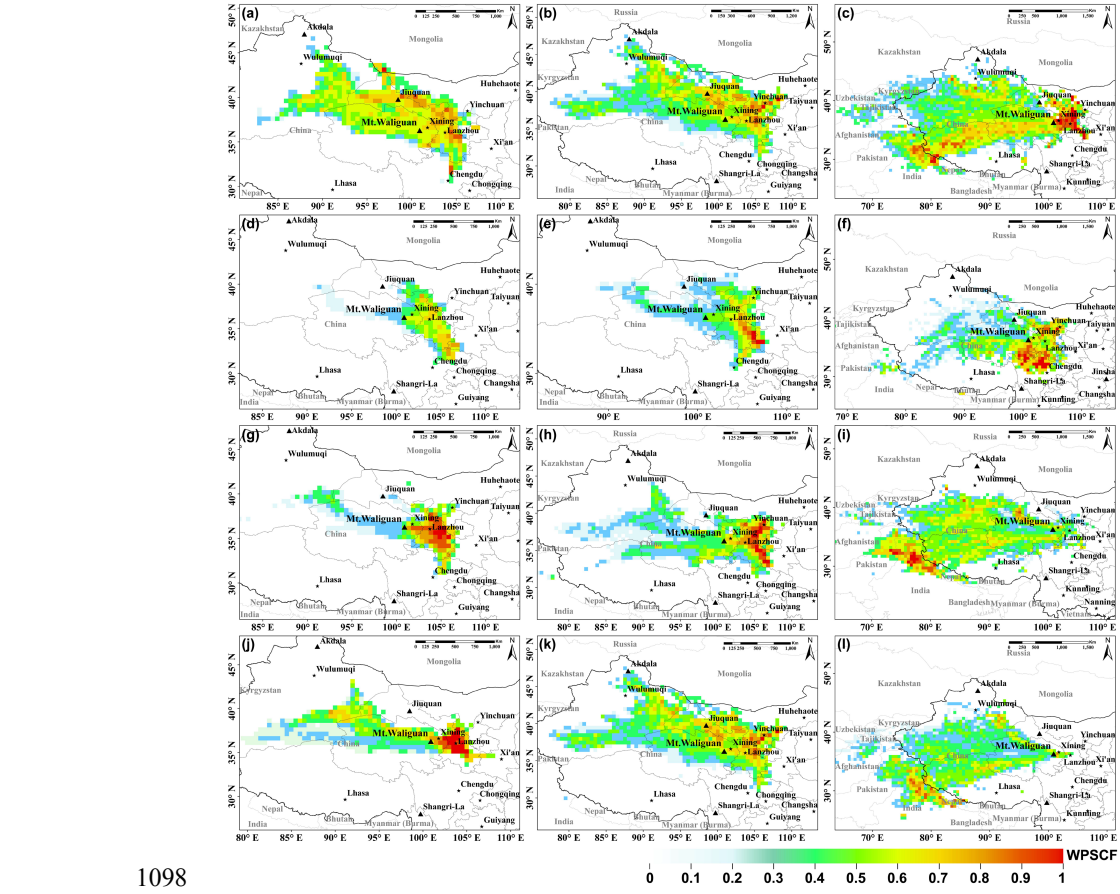

Figure 6. Geographical distribution of weighted potential source of CH_4 in different periods over 1994-2017 at WLG station. The gradient color shows strong levels of potential source regions in different seasons, i.e. spring (a, b, c), summer (d, e, f), autumn (g, h, i) and winter (j, k, l), and different periods, i.e. 2004-2007 (a, d, g, j), 2008-2012 (b, e, h, k) and 2013-2017 (c, f, i, l).

https://doi.org/10.5194/acp-2020-481
Preprint. Discussion started: 29 July 2020

Atmospheric Chemistry and Physics Discussions

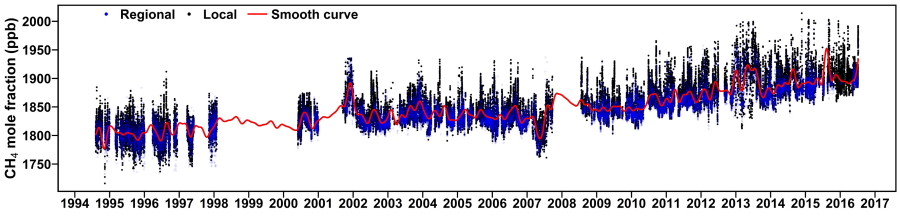

Figure 7. Filtered hourly CH_4 data series from 1994 to 2017 at WLG station. The blue points with transparency represent regional events. The black points are the filtered local events. The red lines are calculated smooth values to the regional data by curve-fitting routine of Thoning et al. (1989).

https://doi.org/10.5194/acp-2020-481
Preprint. Discussion started: 29 July 2020

Atmospheric Chemistry and Physics Discussions

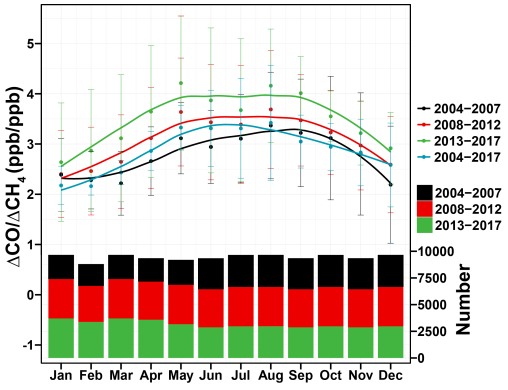

Figure 8. Average seasonal variation of $\Delta CO/\Delta CH_4$ slopes in different periods over 2004-2017 at WLG station. The error bars show the standard deviation of the monthly averages. The vertical bars are the monthly numbers of data in different periods.

https://doi.org/10.5194/acp-2020-481
Preprint. Discussion started: 29 July 2020

Atmospheric Chemistry and Physics Discussions

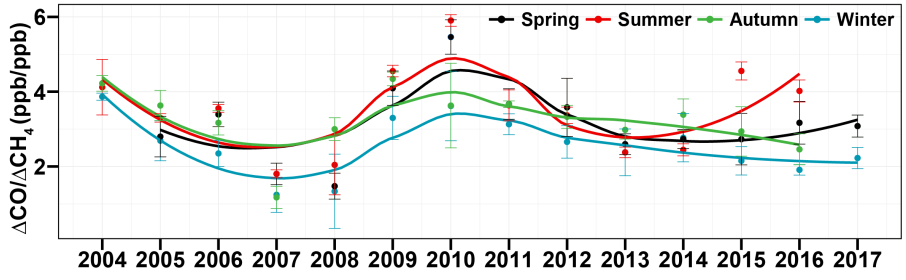

1111

1112 **Figure 9.** Long-term trend of $\Delta CO/\Delta CH_4$ slopes over 2004-2017 at WLG station.

https://doi.org/10.5194/acp-2020-481
Preprint. Discussion started: 29 July 2020

Atmospheric Chemistry and Physics Discussions

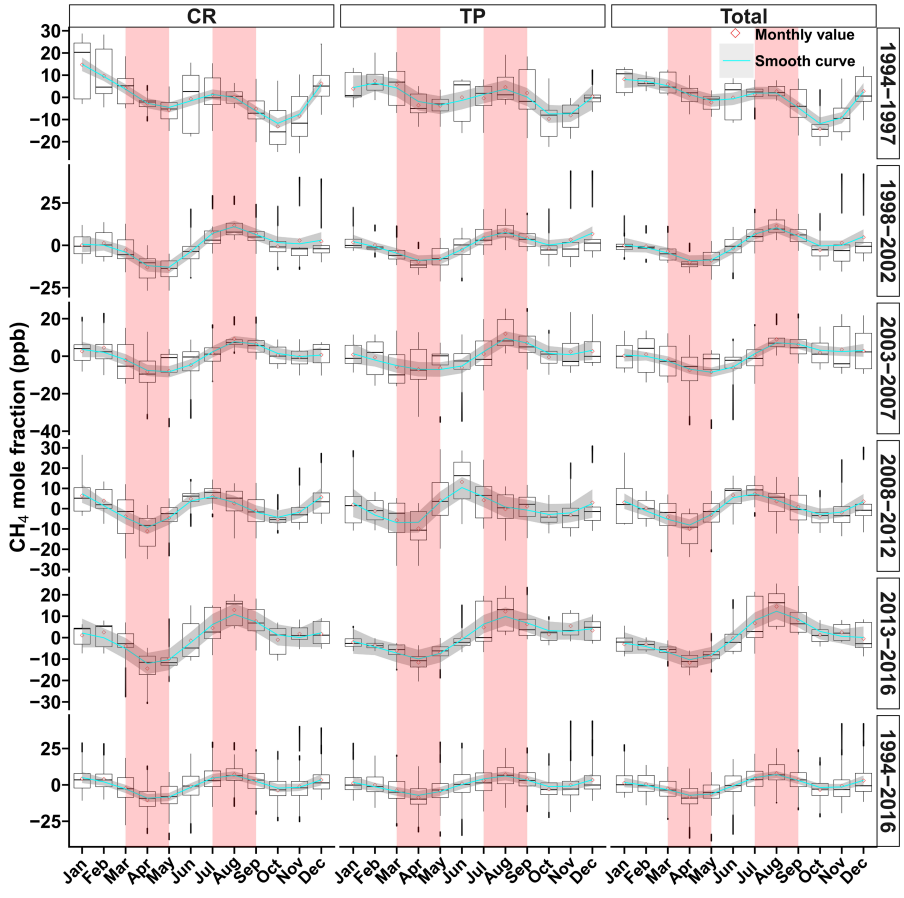

Figure 10. Monthly variations of regional CH_4 mole fractions from 1994 to 2016 at WLG station. The 'CR', 'TP' and 'Total' represents the measurements from the City Regions, the Tibet Plateau and the original total regional records, respectively. The box respectively shows the 25th percentile, the median and the 75th percentile from bottom to top. The bottom and the top whisker respectively reaches the minimum and 1.5 times the IQR (interquartile range). The black points are identified as outliers. The red squares are the averages. The cyan lines are the smooth curve of averages using the method of loess (Local Polynomial Regression Fitting). The gray bands are the 95% confidence interval of smooth curve.

https://doi.org/10.5194/acp-2020-481
Preprint. Discussion started: 29 July 2020

Atmospheric Chemistry and Physics Discussions

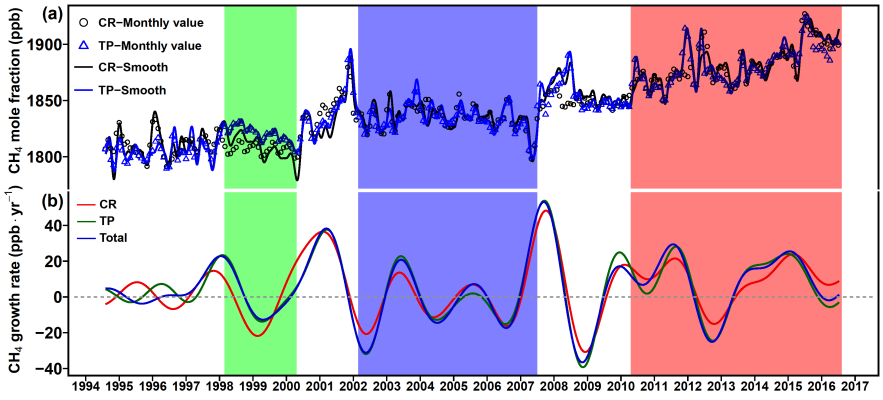

Figure 11. The top panel (a) shows the smooth curve and monthly values of CH_4 mole fraction in the City Regions (CR) and the Tibet Plateau (TP) during 1994-2016 at WLG station. The bottom panel (b) is the annual growth rates of atmospheric CH_4 records from CR, TP as well as the total regional time series (Total). The growth rates are calculated from the first derivative of trend curves. The smooth curve and the trend is calculated by the method of Thoning et al. (1989).

https://doi.org/10.5194/acp-2020-481
Preprint. Discussion started: 29 July 2020

Atmospheric Chemistry and Physics Discussions

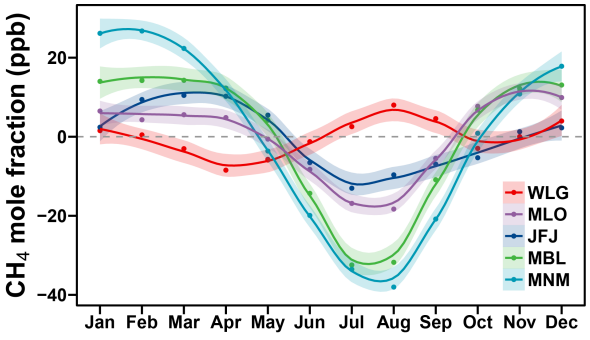

1128

1129 **Figure 12.** The seasonal cycles of atmospheric CH_4 observed over 1994-2017 at WMO/GAW global

1130 stations of Mauna Loa (MLO), Jungfraujoch (JFJ), Minamitorishima (MNM) and Mt.Waliguan

1131 (WLG) in the northern hemisphere. The data of other sites (except WLG) are from WDCGG. The

1132 data in the marine boundary layer (MBL) are from NOAA / ESRL lab at the similar latitude to WLG.